공학석사 학위논문

Study on a Fatigue Analysis for a Vertical Tube Considering Nonlinearity of Morison Force

수직 튜브에 작용하는 모리슨 하중의 비선형성을 고려한 피로 해석에 관한 연구

2017 년 2 월

서울대학교 대학원

조선해양공학과

감 민 주

Study on a Fatigue Analysis for a Vertical Tube Considering Nonlinearity of Morison Force

지도 교수 장 범 선

이 논문을 공학석사 학위논문으로 제출함

2017 년 2 월

서울대학교 대학원
조선해양공학과
감 민 주

감민주의 공학석사 학위논문을 인준함

2017 년 2 월

위 원 장 노 명 일 (인)

부위원장 장 범 선 (인)

위 원 김 낙 완 (인)

Abstract

Study on a Fatigue Analysis for a Vertical Tube Considering Nonlinearity of Morison Force

Gam Minju

Department of Naval Architecture and Ocean Engineering

The Graduate School

Seoul National University

There are two types of offshore structures subjected to Morison force; single pile type and multi pile type which is complex of single piles. Among them, seawater caisson attached to FPSO (Floating Production Storage Offloading), which is vertical single type tube, is selected as the object of this study. Fatigue analysis for the seawater caisson should be performed at the caisson-FPSO hull joint since fatigue failure occurs at the joint, not at the caisson itself in many

cases. Local hotspot stress induced by Morison force and global hotspot stress by hull girder load are applied to the supporting structure of the caisson. Therefore, both stresses should be properly combined in the fatigue analysis. In addition, due to relative velocity squared in drag term, nonlinearity of Morison force should be taken into account as well.

In actual situation, nonlinearity of Morison force and effects by motion of structure and wave elevation should be included in fatigue analysis for floating offshore structure such as FPSO. In time domain method, all of them can be considered, but it is impossible to consider in frequency domain method. For that reason, time domain method is relatively accurate, but it takes a long time to calculate. Therefore, this study began with the necessity of developing a method that has the merits of both methods.

Procedures and in-house codes of a time domain method and two frequency domain methods are developed in this study. Through time domain method, called RFC method, a close approximation to the exact solution can be calculated by considering all factors. In the first frequency domain method, called spectral method, only nonlinearity of Morison force is considered. In the second frequency domain method, called spectral method with stretching, an attempt is made

to take into account stretching effect by wave elevation.

In time domain method, relative velocities above MWL (Mean Water Level) can be obtained using stretching method; vertical stretching and extrapolation stretching. To keep relations between relative velocities at each depth, superposition is applied. In addition, consideration of time dependent varying submerged range, which has an influence on fatigue damage, is included. In frequency domain method, linearization coefficient is calculated using two stochastic linearization methods; one is for narrow-band wave spectrum and one is for wide-band wave spectrum. Furthermore, wave elevation is taken into account using stretching method.

In the results section, there are five categories. The first is verification of in-house code and it is performed using commercial software. Then, using developed code, it is figured out that how well linearization coefficient approximates nonlinear Morison force. In the next category, the results of two linearization coefficient calculation methods are compared. The other two categories are conducted to verify spectral method with stretching. First, which of the two factors, motion effect and stretching effect, has a dominant influence on fatigue damage is found, and then, effectiveness of the suggested method verified.

Keywords : Fatigue analysis, Vertical tube, Nonlinearity of Morison force, Stretching effect, Time domain method, Frequency domain method, Stochastic linearization coefficient

Student Number : 2015-21158

Contents

List of Figures

List of Tables

NOMENCLATURE

DOF	= Degree of Freedom
FPSO	= Floating Production Storage Offloading
MWL	= Mean Water Level
PDF	= Probability Density Function
RAO	= Response Amplitude Operator
RFC	= RainFlow Counting
a	= Fluid particle acceleration
$a_j(t)$	= Time history of relative acceleration for irregular wave at j^{th} depth
$\bar{a}$	= Parameter of one−slope SN curve
$\bar{a}_1, \bar{a}_2$	= Parameters of two−slope SN curve
A	= Projected area of the tube = Amplitude of incoming wave
A_i	= Amplitude of i^{th} regular component wave
$A_{most\ probable}$	= Most probable wave amplitude
A_s	= Significant wave amplitude
$\bar{A}$	= Mean wave amplitude
$\bar{A}_{1/10}$	= Amplitude of the highest 10% of waves
C_A	= Added mass coefficient
C_D	= Drag coefficient in the Morison equation
C_M	= Inertia coefficient in the Morison equation
d	= Diameter of the tube
D	= Accumulated fatigue damage considering all sea states and heading angles
D_{ij}	= Fatigue damage ratio for ith sea state and jth heading angle

$E[D]$	= Expected fatigue damage based on nonlinear PDF
$E[D]_{lin}$	= Expected fatigue damage based on linearized PDF
F	= Morison force
F_D	= Drag force
F_I	= Inertia force
F_j	= Morison force at j^{th} depth
F'	= Approximate Morison force
F'_k	= Approximate Morison force at k^{th} location
$\hat{F}_*$	= Peak value of force divided by the standard deviation of force
$\|H\|$	= Amplitude of response
H_{Im}	= Imaginary part of response
H_{Re}	= Real part of response
H_s	= Significant wave height
i	= Index for regular component wave
j	= Index for water depth defined in the global coordinate = Index for heading angle
k	= Index for location from the bottom of the tube defined in the local coordinate = The number of stress blocks
K	= Drag−inertia parameter
$l(t)$	= Time history of the submerged length of the tube
m	= Parameter of one−slope SN curve
m_1, m_2	= Parameters of two−slope SN curve
m_0	= 0^{th} moment of wave spectrum

m_{0ij}, m_{2ij}	= 0^{th} and 2^{nd} moment of the combined principal stress spectrum for i^{th} sea state and j^{th} heading angle
m_{k}	= kth moment of the spectrum
n	= The number of regular waves
n_i	= The number of stress cycles in stress block i
N_i	= The number of cycles to failure at the constant stress range $\Delta\sigma_i$
$p(\xi)$	= PDF of all maxima ξ
$p_F(\hat{F}_*)$	= PDF of normalized peak force
$p_x(\hat{x}_*)$	= PDF of normalized peak stress
p_{ij}	= Occurrence probability for i^{th} sea state and j^{th} heading angle
Q	= Least square value
R	= Response induced by incoming wave
Re	= Real part
$S(\omega_i)$	= Wave spectral energy density for angular frequency
S_0	= Stress range at which the slope of SN curve changes
SF	= Stress influence factor
SF_k	= Stress influence factor at k^{th} location
$S_v(\omega)$	= Relative velocity spectrum
T_d	= Design life expressed in seconds
T_z	= Zero up−crossing period
$u_j(t)$	= Time history of relative velocity for irregular wave at j^{th} depth
$u_{Re,ij}, u_{Im,ij}$	= Real, imaginary part of relative velocity

	RAO for i^{th} regular component wave at j^{th} depth
v	= Fluid particle velocity
V	= Volume of the tube
$VD(t)$	= Time history of vertical displacement at the bottom of the tube
$VD_{Re,i}, VD_{Im,i}$	= Real, imaginary part of vertical displacement RAO for i^{th} regular component wave
$VL(t)$	= Time history of vertical location of the bottom of the tube
x	= x coordinate value in the global coordinate
$x(\mathrm{t})$	= Gaussian wide−band and zero−mean process
$\hat{x}_*$	= i^{th} stress peak amplitude
X	= Linearization coefficient
y	= y coordinate value in the global coordinate
z	= z coordinate value in the global coordinate
$\gamma(a,z)$	= Lower incomplete gamma function
$\Gamma(a,z)$	= Upper incomplete gamma function
$\Gamma(a)$	= Ordinary gamma function
Δh	= Discretized height of the tube
$\Delta\sigma_i$	= Constant amplitude stress range blocks
$\Delta\omega$	= Angular frequency interval
ε	= Bandwidth parameter of wave spectrum
$\zeta(t)$	= Time history of irregular wave elevation
$\eta_1, \eta_2, \eta_3, \eta_4, \eta_5, \eta_6$	= Surge, sway, heave, roll, pitch, yaw at the origin of global coordinate
ν_{ij}	= Average zero crossing frequency of the

	combined principal hotspot stress for i^{th} sea state and j^{th} heading angle
ξ	= Displacement = Maxima
ξ_1, ξ_2, ξ_3	= x, y, z directional displacement for a specific point
ξ_{re}, ξ_{im}	= Real, imaginary part of displacement
$\dot{\xi}$	= Velocity
$\dot{\xi}_{re}, \dot{\xi}_{im}$	= Real, imaginary part of velocity
ρ	= Seawater density
σ	= Standard deviation of the fluid particle velocity
σ_1, σ_2	= First, second principal stress
$\sigma_{glo}(t)$	= Time history of global hotspot stress
$\sigma_{glo_{Re,i}}, \sigma_{glo_{Im,i}}$	= Real, imaginary part of the global stress RAO for i^{th} regular wave component
$\sigma_{loc}(t)$	= Time history of total local hotspot stress
$\sigma_{loc,k}(t)$	= Time history of contribution of the Morison force at k^{th} location to local hotspot stress
σ_u	= Standard deviation of relative velocity at a specific point
σ_x	= x directional normal stress = Standard deviation of stress response
σ_y	= y directional normal stress
τ_{xy}	= Shear stress in xy plane
v	= Fluid particle velocity
$\phi_{difference\ by\ depth}$	= Phase angle between MWL and the specified depth
$\phi_{response}$	= Phase angle between incoming wave and

	response
	= Phase angle between the regular wave and relative velocity at MWL
ϕ_{wave}	= Phase angle of a regular wave
$\emptyset_{wave,i}$	= Randomly generated phase angle of i^{th} regular component wave
ω	= Angular frequency of incoming wave
ω_i	= Angular frequency of i^{th} regular component wave
ω_{mv}	= Mean value of zero crossing frequency of the relative velocity normal to the tube

1. Introduction

1.1. Research Background

There are two types of offshore structures subjected to Morison force; single pile type and multi pile type which is complex of single piles. In the first type, there is seawater caisson attached to FPSO which is used to suck seawater. In the second type, there are jack-up rig, jacket structure, and bracing in semi-submersible, etc. Among them, seawater caisson, which is the simplest form, is selected as the object of this study.

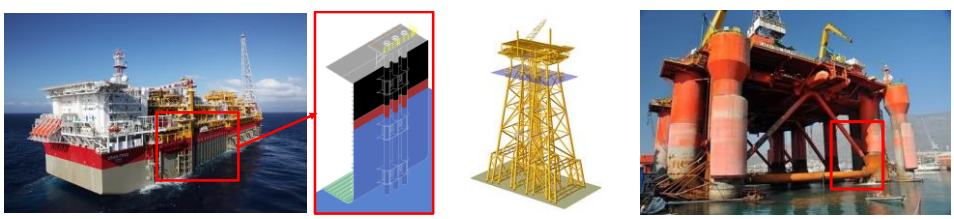

(a) (b) (c)

Fig. 1 Offshore structures subjected to Morison force
(a) seawater caisson attached to FPSO (b) jacket structure
(c) bracing in semi-submersible

Fatigue analysis for the seawater caisson attached to FPSO should be performed at the caisson-FPSO hull joint since fatigue failure at the caisson occurs more at the joint than at the caisson itself. The supporting structure of the caisson is subjected to drag force and inertia force defined by the Morison equation. It is also affected by

hull girder bending. Therefore, local hotspot stress induced by Morison force and global hotspot stress by hull girder load should be properly combined in the fatigue analysis. What should be noted here is that there is nonlinearity in Morison force since drag term is nonlinear due to relative velocity squared. For this reason, nonlinearity of Morison force needs to be considered in fatigue analysis for the caisson.

1.2. Research Status

If Morison force is nonlinear (see Eq.[1]), analysis in frequency domain is not possible since assumption about linear relation is broken. Thus, many studies use linearization of Morison force (see Eq.[2]) to perform the analysis in frequency domain. In Eq.[2], X means linearization coefficient.

$$F = F_I + F_D = \rho V C_M a + \frac{1}{2}\rho C_D A v|v|$$

[1]

$$F = \rho V C_M a + \frac{1}{2}\rho C_D A v X$$

[2]

Several types of methods have been used to calculate the linearization coefficient for the drag term in the Morison equation.

Among them, a fundamental and basic one is the equivalent linearization method proposed by Borgman(1972). In this method, the least square approach to minimize the error between the nonlinear formula of drag force and the linearized one is adopted. Considering that the regular wave elevation is a Gaussian random process, the particle velocity of wave can be also regarded as a Gaussian process. Therefore, the least square value Q is expressed as shown in the following formula. X is the linearization coefficient and σ is the standard deviation of the particle velocity, v.

$$\mathrm{Q} = \int_{-\infty}^{\infty} (v|v| - Xv)^2 \left[\frac{\exp\left(-\frac{v^2}{2\sigma^2}\right)}{\sqrt{2\pi}\sigma} \right] dv$$

[3]

Using this formula, the coefficient can be defined as follows.

$$X = \sigma \sqrt{\frac{8}{\pi}}$$

[4]

The approach of Borgman has been widely used and the expected fatigue damage calculated using this coefficient is nearly the same as the value calculated by the nonlinear form if the inertia term is dominant. On the other hand, if the drag term is governing, this approach results in a considerable difference as compared to the

fatigue damage calculated using nonlinear formula (Tickell, 1977).

To overcome this limitation, Brouwers and Verbeek (1983) suggested a method to evaluate the ratio between the fatigue damages calculated using the linearization coefficient by Borgman and the one using the nonlinear Morison equation. By multiplying this value with the linearization coefficient by Borgman, a more precise linearization coefficient can be calculated. The method is based on the assumption that, since the fatigue damage is proportional to the power of expected value of the peak force, the expectation value of the power of peak force calculated by the nonlinear form should be equal to that by the linearization form. The analytic formula to estimate the ratio introduced a new parameter K which represents the relative magnitude of the drag force to the inertia force in the Morison equation.

Borgman derived PDF (Probability Density Function) of peak force under the assumption that wave spectrum is narrow-band process. After that, Tung (1974), Tickell, and Moe and Crandall (1978) derived PDF of peak force which can be applied to wide-band wave spectrum. Linearization coefficient calculation method for narrow-band wave spectrum is developed by Brouwers and Verbeek and method for wide-band wave spectrum is not suggested yet.

Both equivalent and stochastic linearization method are used in

frequency domain. Since frequency domain method is less accurate and has several limitations, time domain method has appeared; Karadeniz (1994) and Choi et al. (1995).

1.3. Research Objective

Characteristics of frequency and time domain method are presented in Table 1. In frequency domain method, Morison force should be linearized since nonlinearity cannot be considered in frequency domain. In addition, motion of structure and wave elevation cannot be taken into account. Thus, the accuracy of frequency domain method is relatively low due to those reason. The advantage of the method is that computational time for the analysis is short. The advantages and disadvantages of time domain method are opposite to those of frequency domain method. This study began with the necessity of developing a method that has the merits of both methods.

In this study, procedures and in-house codes of a time domain method and two frequency domain methods are developed. Through the time domain method, called RFC method, a close approximation to the exact solution can be calculated by considering all factors listed in Table 1; nonlinearity of Morison force, motion of structure, and wave elevation. In the first frequency domain method, called spectral method, only nonlinearity due to Morison force is considered. In the

second frequency domain method, called spectral method with stretching, an attempt is made to take into account stretching effect by wave elevation. The procedures and details of each method are described in section 2 to section 4.

Table 1 Characteristics of frequency and time domain method

	Frequency domain method	Time domain method
Type of Morison force	Linearized	Nonlinear
Motion of structure	X	O
Wave elevation	X	O
Accuracy	Low	High
Computational time	Short	Long

Furthermore, linearization method for wide-band wave spectrum is suggested in this research since it has not developed yet as described in section 1.2.

2. Time Domain Method

2.1. Overall Procedure of Time Domain Method

Time domain method is developed to cover the nonlinearity of the Morison equation, motion of structure and wave elevation. For an accurate calculation, phase differences of wave particle velocities along the tube should be appropriately taken into account. Fig. 2

depicts the fatigue analysis procedure in the time domain. It consists of the following three parts.

Part 1 aims to calculate all RAOs (Response Amplitude Operator) to be used as input to Part 2 through the hydrodynamic and the global strength analyses in DNV-WADAM (DNVGL,2013) and DNV-SESTRA (DNVGL,2013). RAOs for a set of fluid particle velocities along the tube and 6 DOF (Degree of Freedom) motions are calculated by the hydrodynamic frequency domain analysis. For each depth, fluid particle velocity and motion RAO are used to generate RAOs of relative velocity. Meanwhile, the global hotspot stress RAO is calculated using the global strength FE analysis.

The goal of Part 2 is to generate time history of the combined principal hotspot stress to be used for the fatigue damage calculation. Part 2 is conducted using the in-house code. In the first step of Part 2, for a representation of an irregular wave for a sea state, a sufficiently large number of regular component waves are defined from a wave spectrum corresponding to the sea state. For a regular wave with a specific frequency, the wave amplitude is defined from the corresponding wave spectral energy density and its phase angle is randomly generated in MATLAB. For an efficient treatment of various phase angles, a complex form is used for all responses. In

the next step, time histories of relative velocity and three components of global stresses $(\sigma_x, \sigma_y, \tau_{xy})$ are generated by combining all sinusoidal function. Time histories of local hotspot stresses are transformed from time history of the Morison load using the stress influence factor. Nonlinearity of drag term can be considered in time domain. Local hotspot stress also has three components. By combining local hotspot stress and global stress separately for three components, the time histories of the three combined component stresses are obtained. In the last step of Part 2, time history of the combined principal hotspot stress is calculated from three combined stress components.

In Part 3, fatigue damage is calculated from the time history of the combined principal hotspot stress. The result of Part 3 is close to the exact solution and it is used for verification of the two-types of frequency domain method.

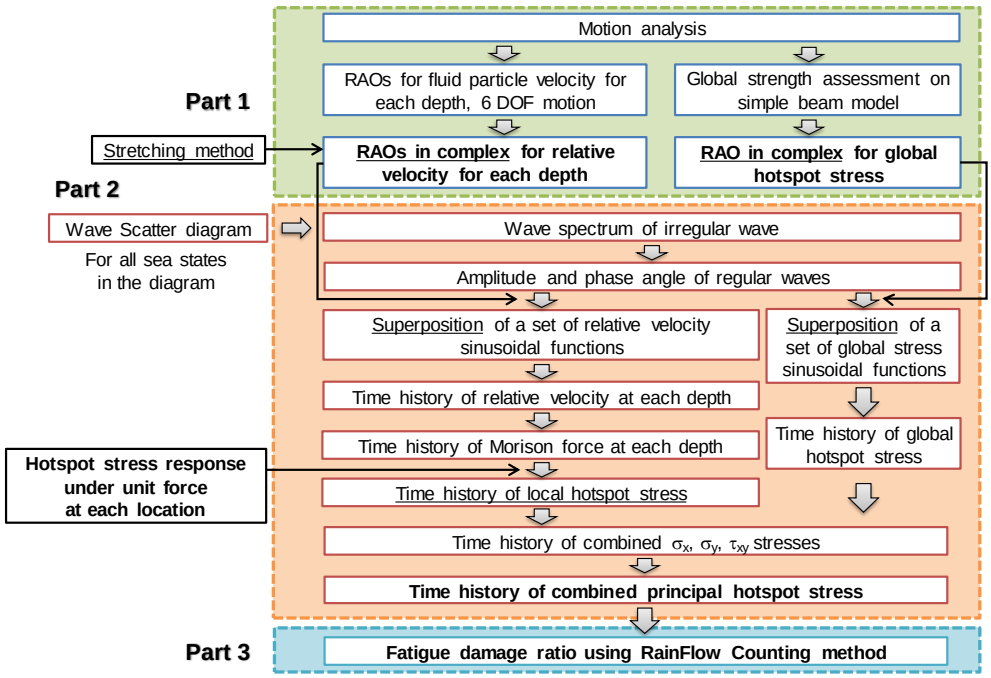

Fig. 2 Time Domain Method Procedure

Time domain method is named RFC method in this study since fatigue is calculated using RainFlow Counting method.

2.2. Key Point of Time Domain Method

2.2.1. Stretching Method

In view of the assumption of small wave amplitude, fluid particle velocity above MWL cannot be calculated in the linear wave theory. Thus, relative velocity RAO above water line should be extrapolated using relative velocity RAO below water. There are three types of stretching methods: vertical stretching, extrapolation stretching, and Wheeler stretching (Wheeler, 1969). Fig. 3 shows the difference

between the linear wave theory and the three types of stretching methods. Vertical stretching is the simplest. This method assumes that the velocity above water is constant and equal to the velocity at the MWL. Extrapolation stretching calculates velocity above water using a linear extrapolation which is drawn by one point and slope. The point is velocity at the MWL and the slope is tangent at that point. Wheeler stretching uses a newly defined z to calculate the velocity for the whole depth. As can be seen from Fig. 3, Wheeler stretching and extrapolation stretching underestimate and overestimate velocity, respectively. In the present study, two conservative methods, vertical stretching and extrapolation stretching, are adopted in the in-house code. The stretching is made separately for real and imaginary parts of relative velocities.

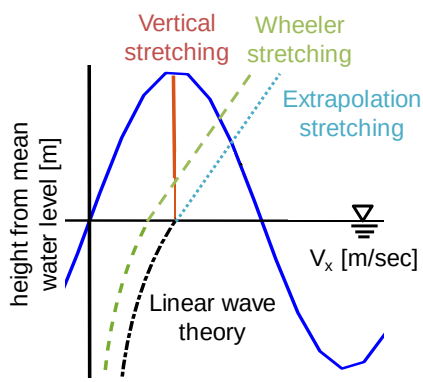

Fig. 3 Comparison of different stretching methods

2.2.2. Complex Expression

To generate time history of response using its RAO and wave information, following expression is introduced:

$$R = A \cdot Re\left\{|H| \cdot e^{i(\omega t + \phi_{response})}\right\}$$

[5]

where A and ω are amplitude and angular frequency of incoming wave, R is response induced by incoming wave like relative velocity and global stress, $|H|$ is amplitude of response, and $\phi_{response}$ is phase angle between incoming wave and response. Amplitude and phase angle of response can be defined in complex from as follows:

$$H = H_{Re} + iH_{Im}$$

$$\phi_{response} = tan^{-1}\frac{H_{Im}}{H_{Re}}$$

[6]

If applying Euler's formula to [5]:

$$R = A \cdot |H| \cdot \cos(\omega t + \phi_{response})$$

[7]

If applying trigonometric function formula to [7]:

$$R = A \cdot H_{Re} \cdot \cos \omega t - A \cdot H_{Im} \cdot \sin \omega t$$

[8]

Phase angle between incoming wave and response can be considered using both Eq.[7] and Eq.[8]. The difference between Eq.[7] and Eq.[8] is that; the first one is using amplitude and phase angle, and the second one is using real and imaginary parts. In this research, Eq.[8] is chosen between two methods because phase angle differences can be taken into account automatically when using Eq.[8].

An example below can explain the reason of selecting Eq.[8] in detail. When Eq.[7] is used to calculate the time history of relative velocity at a certain depth, there are four phase angles which should be considered; phase angle of a regular wave (ϕ_{wave}) consisting an irregular wave, phase angle between the regular wave and relative velocity at MWL ($\phi_{response}$), and phase angle between MWL and the specified depth ($\phi_{difference\ by\ depth}$). Then, Eq.[7] is rewritten as follows.

$$R = A \cdot |H| \cdot \cos\left(\omega t + \phi_{wave} + \phi_{response} + \phi_{difference\ by\ depth}\right)$$

[9]

Meanwhile, if using the definition of real and imaginary of relative velocity, there is no need to introduce these phase angles separately

because the information of phase angles is automatically covered by the complex expression. Therefore, using the complex form (Eq.[8]) is more convenient than using amplitude and phase angle (Eq.[7]).

Here, Eq.[8] does not include the phase angle of a regular wave. Thus, Eq.[8] should be rewritten as follows.

$$R = A \cdot H_{Re} \cdot \cos(\omega t + \phi_{wave}) - A \cdot H_{Im} \cdot \sin(\omega t + \phi_{wave})$$

[10]

2.2.3. Superposition Method

Relative velocity spectrum at each depth can be obtained from the hydrodynamic analysis and the time history of relative velocity for irregular wave can be generated directly by applying inverse fast Fourier transform to the relative velocity spectrum. However, this method randomly generates time histories of relative velocity for each water depth and the timewise relations of relative velocities at different depths cannot be realized. The relation can be maintained only when they are generated for the same regular waves and are superposed for an irregular time history. This method is named superposition method.

2.2.4. Time Dependent Varying Submerged Range

In a floating structure, the submerged range of the tube varies over time due to the vertical motion of the structure and wave elevation. Change of submerged range due to the first reason can be considered using the time history of vertical location at the bottom of the tube. Change due to the second one can be taken into account using stretching for relative velocity above MWL. In this research, two effects that influence on the fatigue damage; motion effect and stretching effect. Motion effect and stretching effect mean effect on fatigue damage by motion of structure and wave elevation, respectively.

2.3. Procedure Description of Time Domain Method

2.3.1. Part 1 – Generation of RAOs

To create the time histories of local hotspot stress and global hotspot stress, three kinds of RAOs are necessary: (1) vertical displacement RAO at the bottom of the tube; (2) relative velocity RAOs at each depth; and (3) global hotspot stress RAOs. RAOs for fluid particle velocity for each depth and 6 DOF motions are obtained through the hydrodynamic analysis. Then, RAOs for relative velocity at each depth and vertical displacement are calculated by the in-

house code.

Generation of vertical displacement RAO

Vertical displacement RAO can be derived using the following formula:

$$\xi_3 = \eta_3 + y\eta_4 - x\eta_5$$

[11]

where ξ_3 is z directional displacement for a specific point, η_3, η_4, η_5 are heave, roll, and pitch at the origin of global coordinate, respectively, x, y are x, y are the coordinate values of the point in the global coordinate.

Generation of relative velocity RAOs at each depth

To calculate local hotspot stress considering the wave heading angle, local hotspot stress should be generated separately for x and y directional horizontal relative velocities. For this purpose, structural displacement and velocity at a point of interest should be calculated first using the following formulas.

$$\xi_1 = \eta_1 + z\eta_5 - y\eta_6$$

$$\xi_2 = \eta_2 + x\eta_6 - z\eta_4$$

[12]

where ξ_1, ξ_2 are x, y directional displacement at a specific point, η_1, η_2, η_6 are surge, sway, and yaw at the origin of global coordinate, respectively, z is z coordinate value in the global coordinate.

Velocity RAO can be derived from the corresponding displacement RAO, as shown below.

$$\dot{\xi} = i\omega\xi$$

[13]

where $\dot{\xi}$ is velocity. The above formula can be written in a complex form (see below).

$$\dot{\xi} = i\omega\xi = i\omega(\xi_{re} + i\xi_{im}) = -\omega\xi_{im} + i\omega\xi_{re} = \dot{\xi}_{re} + i\dot{\xi}_{im}$$

[14]

Structural velocity RAOs are generated for each depth. Then, horizontal relative velocity can be calculated by the subtracting the structural velocity from the fluid particle velocity measured at each depth from the hydrodynamic analysis. Since the submerged range of the tube changes over time due to the structure motion, relative velocity RAOs for a sufficiently deep depth beyond the tube bottom should be generated in the hydrodynamic analysis. Relative velocity RAOs above the MWL can be obtained using stretching method

introduced in 2.2.1.

Generation of global stress RAO

Global hotspot stress RAOs for three components $(\sigma_x, \sigma_y, \tau_{xy})$ are calculated using the global strength analysis subject to wave loads transferred from the hydrodynamic analysis for unit regular waves of different heading angles and angular frequencies. The effect of hull girder load on the vertical tube could be negligible. However, a tube supporting structure attached on the side shell is significantly affected by the hull girder load, as well as the local Morison load. Fig. 14 (b) and (c) show an example of such supporting structure.

2.3.2. Part 2 – Generation of Time History of Combined Principal Hotspot Stress

In Part 2, time history of principal stress at hotspot is generated at the final step. Steps are described in further detail below.

Definition of an irregular wave for a sea state

In the linear wave theory, an irregular wave can be expressed as a superposition of multiple regular waves. For a sea state, amplitude of each regular wave is defined using the corresponding wave

spectrum (see Eq.[15]).

$$\zeta(t) = Re\left\{\sum_{i=1}^{n} A_i e^{i(\omega_i t + \emptyset_{wave,i})}\right\} = \sum_{i=1}^{n} A_i \cdot \cos(\omega_i t + \emptyset_{wave,i})$$

$$A_i = \sqrt{2 \cdot S(\omega_i) \cdot \Delta\omega}$$

[15]

where n is the number of regular waves. $S(\omega_i)$ is wave spectral energy density for angular frequency. A_i, ω_i, and $\emptyset_{wave,i}$ are amplitude, angular frequency, and randomly generated phase angle of i^{th} regular component wave, respectively. $\Delta\omega$ is angular frequency interval $(= \omega_{i+1} - \omega_i)$.

Generation of time history of relative velocity

As mentioned above, relative velocity RAO below the water line can be taken from the hydrodynamic analysis and relative velocity RAO above water can be calculated using stretching methods.

When response R is relative velocity at a specific depth, Eq.[10] means a sinusoidal function of relative velocity for a regular wave which is a component of irregular wave. The time history of relative velocity for irregular wave at j^{th} depth can be generated by a superposition of sinusoidal functions of relative velocity for all regular waves.

$$u_j(t) = \sum_{i=1}^{n} A_i \cdot u_{Re,ij} \cdot cos(\omega_i t + \emptyset_{wave,i}) - A_i \cdot u_{Im,ij} \cdot sin(\omega_i t + \emptyset_{wave,i})$$

[16]

where $u_{Re,ij}$ and $u_{Im,ij}$ are real part and imaginary part of relative velocity RAO for i^{th} regular component wave at j^{th} depth, respectively.

Time history of relative velocity at each depth can be generated using Eq.[16]. The relative velocity is separately calculated along x and y directions. As the number of regular waves increases, it can more exactly realize the given wave spectrum; however, it takes too long to generate irregular waves for all sea states in a wave scatter diagram. Here, $n = 640$ is used to define one irregular wave. The number of regular waves is selected by considering both time efficiency and absence of regularity, at the same time. The more regular waves are combined the less regularity is observed but the longer time is necessary for the analysis. When 640 regular waves are used, regularity in irregular wave is rarely found and time for computation is reasonable.

Generation of time history of Morison force

The time history of relative acceleration for irregular wave at j^{th}

depth can be written with the following mathematical expression:

$$a_j(t) = \ddot{u}_j(t) = \sum_{i=1}^{i=n} \{-A_i \cdot \omega_i \cdot u_{Re,ij} \cdot sin(\omega_i t + \emptyset_{wave,i}) - A_i \cdot \omega_i \cdot u_{Im,ij} \cdot cos(\omega_i t + \emptyset_{wave,i})\}$$

[17]

The relative acceleration is also separately calculated along x and y directions. Drag force is calculated from the relative velocity and inertia force is calculated from the relative acceleration. Then, the time history of the Morison load is generated by summing the time histories of drag force and inertia force. It needs to be calculated for a sufficiently deep range at a certain interval–for example, 1m. The nonlinearity of drag term can be taken into account since the Morison equation can be directly used in the time domain calculation (see Eq.[18]).

$$F = F_I + F_D = \rho V C_M a + \frac{1}{2}\rho C_D A u|u|$$

[18]

where F_I, F_D are inertia and drag force, u is relative velocity between the tube and the water particle, a is relative acceleration, seawater density $\rho = 1025kg/m^3$, V is volume of the tube, A is projected area of the tube, C_M is inertia coefficient, and C_D is drag coefficient

Since the target of the fatigue analysis is the vertical tube, the Morison load at j^{th} depth can be expressed as follows (see Eq.[19]).

$$F_j(t) = \rho \frac{\pi d^2 \Delta h}{4} C_M a_j + \frac{1}{2} \rho C_D d \Delta h u_j |u_j|$$

[19]

where d is diameter and Δh is discretized height of the tube.

The Morison load should be separately calculated for x and y directions, since the relative velocities are also separately defined for both directions.

Generation of time history of local hotspot stress

Structure is subjected to local stress by Morison force as much as submerged range. Thus, it should be considered to generate time history of local hotspot stress. In actual situations, submerged range varies due to the motion of structure and wave elevation.

The time history of vertical displacement at the bottom of the tube is generated as follows (see Eq.[20]).

$$VD(t) = \sum_{i=1}^{i=n} A_i \cdot VD_{Re,i} \cdot cos(\omega_i t + \emptyset_{wave,i}) - A_i \cdot VD_{Im,i} \cdot sin(\omega_i t + \emptyset_{wave,i})$$

[20]

where $VD_{Re,i}$ and $VD_{Im,i}$ are real part and imaginary part of vertical displacement RAO for i^{th} regular component wave.

The time history of vertical location at the bottom of the tube is generated by subtracting draft of the tube from the time history of vertical displacement.

$$VL(t) = VD(t) - draft\ \ of\ \ the\ \ tube$$

[21]

The time history of the submerged length of the tube denoted as $l(t)$ can be obtained by subtracting vertical location at the bottom from the time history of wave elevation defined in Eq. [15]. $\zeta(t)$ and $VL(t)$ can be seen in Fig. 4; blue broken line and red line, respectively.

$$l(t) = \zeta(t) - VL(t)$$

[22]

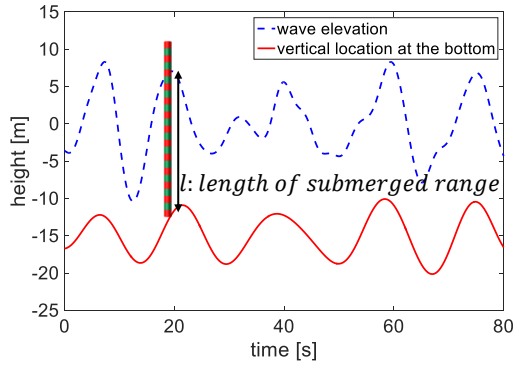

Fig. 4 Submerged range for floating structure

In order to get the time history of local hotspot stress, all contributions by the Morison load at every location to the local

hotspot stress should be integrated over the submerged range. For that purpose, two different coordinate systems are necessary: global coordinate and local coordinate. Notation j indicates j^{th} water depth defined in the global coordinate and k indicates k^{th} location from the bottom of the caisson defined in the local coordinate.

In order to convert the time histories of the Morison loads along the tube to a time history of the local hotspot stress at the supporting structure, the stress influence factor method is applied. A hotspot stress response under a unit load at a location of tube is the stress influence factor at the location. Since the Morison load is divided into x and y directional components and there are three stress components ($\sigma_x, \sigma_y, \tau_{xy}$), a total of six stress influence factors are defined at each location. The Morison load is defined at j^{th} water depth and the stress influence factors at k^{th} location. Thus, the Morison load at k^{th} location needs to be interpolated from pre-defined water depths.

The time history of contribution of the Morison force at k^{th} location to local hotspot stress, $\sigma_{loc,k}(t)$, can be derived by multiplying the Morison load and stress influence factor at k^{th} location as shown below.

$$\sigma_{loc,k}(t) = SF_k \cdot F'_k(t)$$

[23]

where SF_k is the stress influence factor at k^{th} location and F'_k is the approximate Morison force at k^{th} location. Since the locations where SF_k are defined differ from those where F_j are defined, F'_k should be interpolated from two Morison forces defined at the nearest two water depths from k^{th} location (see Fig. 5). In Fig. 5, dash lines indicate water depths at which the Morison forces (F_j) are defined and dots locations for stress influence factors (SF_k). Since their relative locations vary continuously, the Morison force (F'_k) should be approximated from those at dash lines.

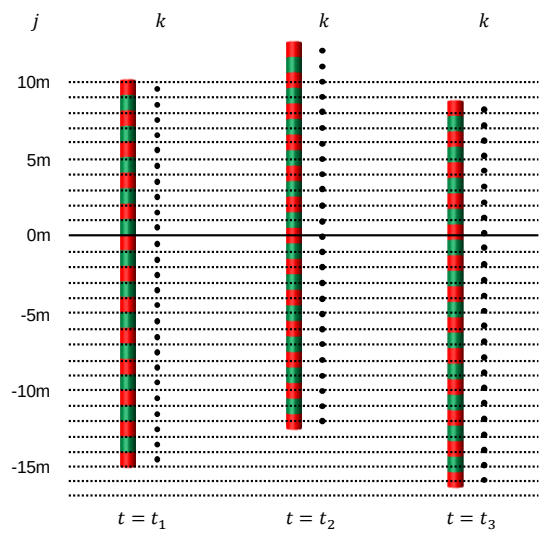

Fig. 5 Location of tube and stress influence factor for floating structure

The local hotspot stress caused by the Morison force should be calculated by collecting the contributions of Morison force within the submerged range. Therefore, the time history of the local hotspot stress can be expressed as shown below (see Eq.[24]).

$$\sigma_{loc}(t) = \int_0^{l(t)} SF(z)\, F'(z,t) dz$$

$$= \sum_{k=1}^{p(t)} SF_k \cdot F'_k(t) + SF_k \cdot F'_k(t) \cdot \{l(t) - \Delta hp(t)\},$$

$$p(t) = round\ \ down\ \ of(\frac{l(t)}{\Delta h})$$

[24]

where $l(t)$ is length of the submerged range, that is distance from wave elevation to the bottom of the tube, and it is function of time. Since $l(t)$ is a rational number, it needs to be introduced by an integer $p(t)$ for a discretized summation. This is separately defined for three stress components ($\sigma_x, \sigma_y, \tau_{xy}$).

Generation of time history of global stress

The method of generating the time history of global stress is similar to that of relative velocity described above. It can be obtained by combining the global stress RAO and a set of regular component waves. It can be written as follows:

$$\sigma_{glo}(t) = \sum_{i=1}^{n} A_i \cdot \sigma_{glo_{Re,i}} \cdot cos(\omega_i t + \emptyset_{wave,i}) - A_i \cdot \sigma_{glo_{Im,i}} \cdot sin(\omega_i t + \emptyset_{wave,i})$$

[25]

where $\sigma_{glo_{Re,i}}$ and $\sigma_{glo_{Im,i}}$ are real and imaginary part of the global stress RAO for i^{th} regular wave component, respectively. This is separately defined for three stress components $(\sigma_x, \sigma_y, \tau_{xy})$.

Generation of time history of combined principal stress

The time histories of three components $(\sigma_x, \sigma_y, \tau_{xy})$ of the combined hotspot stress are calculated by summing the time histories of local $(\sigma_{loc_x}, \sigma_{loc_y}, \tau_{loc_{xy}})$ and global stress components $(\sigma_{glo_x}, \sigma_{glo_y}, \tau_{glo_{xy}})$. The time history of principal stress for the combined stress is obtained using the following principal stress formula:

$$\sigma_{1,2}(t) = \frac{\sigma_x(t) + \sigma_y(t)}{2} \pm \frac{1}{2}\sqrt{\left(\sigma_x(t) - \sigma_y(t)\right)^2 + 4\tau_{xy}(t)^2}$$

[26]

where σ_1 is the first principal stress and σ_2 is the second principal stress. Between the two, the one having the direction normal to crack propagation should be selected.

2.3.3. Part 3 – Calculation of Fatigue Damage

Using the time history of the combined principal hotspot stress generated in Part 2, the fatigue damage ratio is calculated in Part 3. When the long term stress range distribution is expressed by a stress histogram, consisting of a number of constant amplitude stress range blocks $\Delta\sigma_i$ each with a number of stress repetitions n_i, the fatigue damage is calculated by the following formula:

$$\mathrm{D} = \sum_{i=1}^{k} \frac{n_i}{N_i} = \frac{1}{\bar{a}} \sum_{i=1}^{k} n_i \cdot (\Delta\sigma_i)^m$$

[27]

where D is accumulated fatigue damage considering all sea states and heading angles k is the number of stress blocks, n_i is the number of stress cycles in stress block i, N_i is the number of cycles to failure at the constant stress range $\Delta\sigma_i$ and $\bar{a}$, m are SN curve parameters. In the present study, the RFC method is applied to obtain n_i and $\Delta\sigma_i$. If a wave scatter diagram is given, the fatigue damage calculation should be performed for all sea sates in the diagram and summed up with multiplying the corresponding occurrence probability.

3. Frequency Domain Method

3.1. Overall Procedure of Frequency Domain Method

Fig. 6 illustrates the fatigue analysis procedure in the frequency domain. It consists of three parts. Part 1 in the frequency domain is the same as Part 1 in the time domain. In Part 2, linearization coefficient that linearizes the "nonlinear" Morison load is calculated through a stochastic method. In the next step, RAOs for linearized Morison load for each depth are obtained using relative velocity RAOs and linearization coefficient. Relative velocity and the Morison loads are divided into x and y-directional components. Morison load RAOs are transformed to local hotspot stress RAO using the stress influence factors obtained by separate application of x or y directional unit loads along the tube and measuring stress components $(\sigma_x, \sigma_y, \tau_{xy})$. Thus, a total of six stress influence factors are defined for each depth.

By summing the local hotspot stress components and global stress components, three stress component RAOs are generated. The combined principal hotspot stress RAO is calculated from the stress components RAOs. All calculations are made in a complex form. That is, RAOs for real and imaginary parts are used in every step. In the last step in Part 2, combined principal hotspot stress spectrum is

obtained by combining the principal stress RAO and a wave spectrum of a sea state.

In Part 3, fatigue damage is calculated from the combined principal stress spectrum. The result of frequency domain method is compared to the result of time domain method.

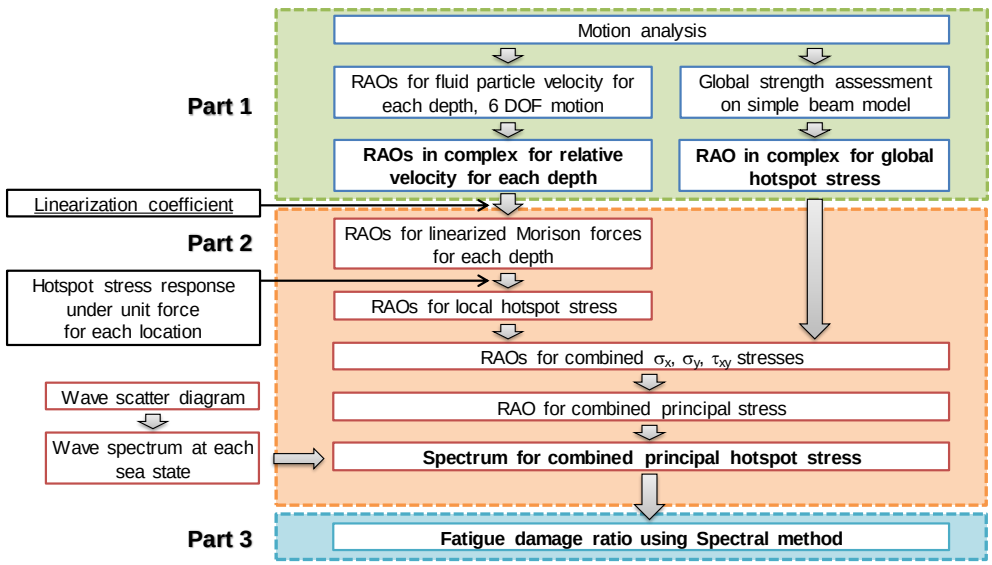

Fig. 6 Frequency Domain Method Procedure

Frequency domain method is named spectral method in this research since fatigue is calculated using spectral method.

3.2. Key Point of Frequency Domain Method

3.2.1. Probability Density Function of Peak Force

PDF of peak force is applied to calculate linearization coefficient

and it varies according to the type of wave spectrum. PDF of peak force for narrow-band wave spectrum was derived by Borgman (1967). PDF for wide-band wave spectrum was derived by Tung (1974), Tickell (1977), and Moe and Crandall (1978). In 3.2.1.2, basic concept of the derivation process of PDF is introduced.

3.2.1.1. Probability Density Function of Wave Height

PDF of all maxima ξ of the Gaussian wide-band and zero-mean process $x(t)$ is as follows (Price, 1974):

$$p(\xi) = \frac{1}{(2\pi m_0)^{1/2}}\left[\varepsilon exp\left(-\frac{1}{2}\frac{\xi^2}{m_0}\frac{1}{\varepsilon^2}\right) + (1-\varepsilon^2)^{1/2}\frac{\xi}{{m_0}^{1/2}}exp\left(-\frac{1}{2}\frac{\xi^2}{m_0}\right)\int_{-\infty}^{\frac{\xi}{{m_0}^{1/2}}\frac{(1-\varepsilon^2)^{1/2}}{\varepsilon}} exp\left(-\frac{1}{2}x^2\right)dx\right]$$

[28]

where ξ is maxima, $p(\xi)$ is PDF of all maxima, m_0 is 0^{th} moment of wave spectrum, ε is bandwidth parameter of wave spectrum defined by Price.

If wave spectrum follows narrow-band process $\varepsilon \to 0$, Eq.[28] becomes Rayleigh distribution as given in Eq.[29].

$$p(\xi) = \frac{\xi}{m_0}exp\left(-\frac{1}{2}\frac{\xi^2}{m_0}\right)$$

[29]

3.2.1.2. Probability Density Function of Peak Force

PDF of peak force is derived using the PDF of wave height introduced in 3.2.1.1 and the relation between wave height and peak force. Borgman derived PDF of peak force for narrow-band wave spectrum using PDF of wave height for narrow-band wave spectrum; Rayleigh distribution. In this paper, PDF of peak force for wide-band spectrum is derived by applying Eq.[28] to the Borgman method since the full equations of PDF are rarely found in the papers of Tung, Tickell, and Moe and Crandall.

3.2.2. Linearization Coefficient Calculation Method

As mentioned above, the Morison equation cannot be directly used in the frequency domain, because the drag term in the equation contains a square of the velocity. For this reason, its linearization using the proper coefficient is necessary in the frequency domain fatigue analysis. The original Morison equation can be linearized as follows.

$$F = \rho \frac{\pi d^2 \Delta h}{4} C_M a + \frac{1}{2} \rho C_D d \Delta h u X$$

[30]

where X is linearization coefficient. In other words, uX is used instead of $u|u|$ in the original equation to linearize the drag term.

Linearization coefficient X is calculated using the theory of Brouwers and Verbeek (1983). The Brouwers and Verbeek method is based on PDF of peak force from narrow-band model by Borgman. They applied drag-inertia parameter K, defined as below, to PDF of peak force.

$$K = \frac{2C_D\sigma_u}{\pi C_M d\omega_{mv}}$$

[31]

where σ_u is standard deviation of relative velocity at a specific point and ω_{mv} is mean value of zero crossing frequency of the relative velocity normal to the tube. The relative velocity spectrum $S_v(\omega)$ using the velocity RAO and the wave spectrum can be calculated. From the spectrum, k^{th} moment of the spectrum m_{k}, σ_u, and ω_{mv} can be calculated.

$$\sigma_u = \sqrt{m_0}, \omega_{mv} = \frac{2\pi}{\overline{T}_z} = \sqrt{\frac{m_2}{m_0}}, m_{\mathrm{k}} = \int_0^\infty S_v(\omega)\omega^k d\omega$$

[32]

PDF of peak force using drag-inertia parameter K can be expressed, in normalized form with respect to standard deviation, as:

$p_F(\hat{F}_*)$ $when$ $0 \le \hat{F}_* \le \frac{1}{2}K^{-1}(3K^2+1)^{-1/2}$

$= 2A\hat{F}_* exp\left[-A\hat{F}_*^{\,2}\right]$

$p_F(\hat{F}_*)$ $when$ $\frac{1}{2}K^{-1}(3K^2+1)^{-1/2} \le \hat{F}_* < \infty$

$$= B exp\left[-B\hat{F}_* + \frac{1}{4}D\right]$$

[33]

where $\hat{F}_*$ is the peak value of force divided by the standard deviation of force ($\hat{F}_* = {\sigma_F}^{-1}\hat{F}$) and $p_F(\hat{F}_*)$ is PDF of normalized peak force. A, B, D in Eq.[33] are defined as below:

$$\mathrm{A} = \frac{1}{2}(3K^2 + 1), \mathrm{B} = \frac{1}{2}(3K^2 + 1)^{\frac{1}{2}}K^{-1}, B = (2K^2)^{-1}$$

[34]

Linearization coefficient can be calculated using the following equation.

$$X = \sqrt{\frac{E[D]}{E[D]_{lin}}} \times \sqrt{\frac{8}{\pi}} \times \sigma_u$$

[35]

where $E[D]$ is expected fatigue damage based on nonlinear PDF and $E[D]_{lin}$ is expected fatigue damage based on linearized PDF.

A common method of calculating the expected fatigue damage $E[D]$ is:

$$E[D] = n\beta {\sigma_x}^{\alpha} \int_0^{\infty} {\hat{x}_*}^{\alpha} p_x(\hat{x}_*) d\hat{x}_*$$

[36]

where n is stress peaks, α, β are material constants, $\hat{x}_*$ is i^{th} stress peak amplitude, σ_x is the standard deviation of stress response, and $p_x(\hat{x}_*)$ is PDF of normalized peak stress. Then, the ratio of two expected fatigue damage is:

$$\frac{E[D]}{E[D]_{lin}} = \frac{\int_0^\infty \hat{x}_*{}^\alpha p_x(\hat{x}_*) d\hat{x}_*}{\int_0^\infty \hat{x}_*{}^\alpha \{p_x(\hat{x}_*)\}_{lin} d\hat{x}_*}$$

[37]

When stress response is linearly related to wave force and it quasi-static in nature, Eq.[37] can be calculated by Eq.[33] and it can be seen as:

$$\frac{E[D]}{E[D]_{lin}} = (3K^2+1)^{-(\alpha/2)}\Gamma^{-1}\left(\frac{\alpha}{2}\right)\left[\gamma\left(\frac{\alpha}{2}, \frac{1}{8K^2}\right) + 2^{1+(\alpha/2)}K^\alpha exp\left(\frac{1}{8K^2}\right)\Gamma\left(\alpha, \frac{1}{4K^2}\right)\right]$$

[38]

where $\Gamma(a)$ is the Gamma function and $\gamma(a,z)$ and $\Gamma(a,z)$ are lower and upper incomplete Gamma functions as defined by Abramowitz and Stegun, respectively.

Linearized coefficient calculation method described above can be applied for narrow-band wave spectrum. Method for wide-band can be derived by using PDF of peak force for wide-band wave spectrum instead of Eq.[33]. It is shown that:

$p_F(\hat{F}_*)$ *when* $0 \le \hat{F}_* \le \frac{1}{2}K^{-1}(3K^2+1)^{-1/2}$

$$= \frac{\varepsilon}{\sqrt{\pi}} C exp\left[-\frac{1}{\varepsilon^2}A\hat{F}_*{}^2\right] + \sqrt{1-\varepsilon^2}A\hat{F}_* exp\left[-A\hat{F}_*{}^2\right]\left[erf\left(C\frac{\sqrt{1-\varepsilon^2}}{\varepsilon}\hat{F}_*\right)+1\right]$$

$p_F(\hat{F}_*)$ *when* $\frac{1}{2}K^{-1}(3K^2+1)^{-1/2} \le \hat{F}_* < \infty$

$$= \frac{\varepsilon}{2\sqrt{\pi}} C\left(a\hat{F}_* - 0.25\right)^{-1/2} exp\left(-\frac{1}{\varepsilon^2} B\hat{F}_* + \frac{1}{4\varepsilon^2} D\right)$$

$$+ \frac{\sqrt{1-\varepsilon^2}}{2} B exp\left(-B\hat{F}_* + \frac{1}{4} D\right)\left[erf\left\{\frac{1}{bc}\left(a\hat{F}_* - 0.25\right)^{1/2} \frac{\sqrt{1-\varepsilon^2}}{\varepsilon}\right\} + 1\right]$$

[39]

C, a, bc in Eq.[39] are defined as below:

$$C = \left(\frac{3K^2+1}{2}\right)^{\frac{1}{2}}, a = (3K^2+1)^{\frac{1}{2}}, bc = \sqrt{2}K$$

[40]

Ratio of two expected fatigue damage for wide-band wave spectrum cannot be expressed as closed form, like Eq.[38] due to the complexity of integrals.

3.3. Procedure Description of Frequency Domain Method

3.3.1. Part 1 – Generation of RAOs

Part 1 in frequency domain method is identical with part 1 in time domain method described in section 2.3.1..

3.3.2. Part 2 – Generation of Combined Principal Stress Spectrum

All calculations in Part 2 are performed separately for real and imaginary parts to consider various phase angles automatically.

Calculation of linearization coefficient

Linearization coefficient is calculated using the method introduced in section 3.2.2 and it is different at each depth along the tube. It is obtained separately for x and y directions.

Generation of linearized Morison force RAOs for each depth

Relative acceleration RAO at j^{th} depth can be derived from the relative velocity RAO (see below).

$$a_j(\omega) = \dot{u}_j(\omega) = i\omega u_j(\omega)$$

[41]

The formula can be written in a complex expression.

$$a_j(\omega) = i\omega u_j(\omega) = i\omega\left(u_{Re,j} + iu_{Im,j}\right) = -\omega u_{Im,j} + i\omega u_{Re,j} = u_{Re,j} + \ u_{re,ij}$$

[42]

Morison force RAOs at j^{th} depth can be calculated using the relative velocity RAOs, the linearization coefficient, and inertia force RAOs as follows.

$$F_j(\omega) = \rho\frac{\pi d^2 \Delta h}{4} C_M a_j(\omega) + \frac{1}{2}\rho C_D d\Delta h|\bar{X}|u_j(\omega)$$

[43]

Morison force RAOs for real and imaginary parts are calculated separately for x and y directions.

Generation of local hotspot stress RAO

In frequency domain method, it is practically impossible to consider the motion of structure like time domain method. Thus, the submerged range of the tube is assumed to be fixed when the local hotspot stress is calculated. In addition, wave elevation above the MWL cannot be also taken into account.

$$\sigma_{loc}(\omega) = \int_0^l SF(z)\, F(z,\omega) dz = \sum_{k=1}^{l/\Delta h} SF_k \cdot F_k(\omega)$$

[44]

Local hotspot stress contributions for each depth are generated by multiplying Morison load RAOs and stress influence factors at the location. Total local hotspot stress RAOs can be calculated by summing up all local hotspot stress contributions below water. Local hotspot stress RAOs are also derived for three stress components $(\sigma_x, \sigma_y, \tau_{xy})$.

Generation of combined principal hotspot stress spectrum

Each of the real and the imaginary parts of three types of stresses, global stress, local hotspot stresses due to x and y directional Morison loads, are added separately. The combined stress has three components: σ_x, σ_y, and τ_{xy}. Combined principal hotspot stress

RAOs for real and imaginary parts can be calculated. The combined principal hotspot stress spectrum is generated by multiplying the amplitude of the combined principal stress square and wave spectrum.

3.3.3. Part 3 – Calculation of Fatigue Damage

Using the combined principal hotspot stress spectrum generated in Part 2, the fatigue damage ratio is calculated in Part 3. When a wave scatter diagram is given, the fatigue damage for one-slope SN curve is given by the following:

$$D = \sum_{\substack{i=1,j=1 \\ \text{all sea states} \\ \text{all headings}}} D_{ij} = \sum_{\substack{i=1,j=1 \\ \text{all sea states} \\ \text{all headings}}} \frac{\nu_{ij} p_{ij} T_d}{\bar{a}} \Gamma\left(1+\frac{m}{2}\right)\left(2\sqrt{2m_{0ij}}\right)^m$$

[45]

where

D_{ij}: fatigue damage ratio for i^{th} sea state and j^{th} heading angle

ν_{ij}: average zero crossing frequency of the combined principal hotspot stress for i^{th} sea state and j^{th} heading angle

p_{ij}: occurrence probability for i^{th} sea state and j^{th} heading angle

T_d: design life expressed in seconds

$\bar{a}$ and m: parameters of one-slope SN curve

m_{0ij}, m_{2ij} : 0^{th} and 2^{nd} moment of the combined principal stress spectrum for i^{th} sea state and j^{th} heading angle

$\nu_{ij}$is defined as follows.

$$\nu_{ij} = \frac{1}{2\pi}\sqrt{\frac{m_{2ij}}{m_{0ij}}}$$

[46]

when a bi-linear or two-slope SN curve is applied, the fatigue damage expression is given as follows:

$$D = \sum_{i=1,j=1}^{\substack{all\ sea\ states \\ all\ headings}} \nu_{ij} p_{ij} T_d \left[\frac{\left(2\sqrt{2m_{0ij}}\right)^{m_1}}{\bar{a}_1} \Gamma\left(1 + \frac{m_1}{2}, \left(\frac{S_0}{2\sqrt{2m_{0ij}}}\right)^2\right) + \frac{\left(2\sqrt{2m_{0ij}}\right)^{m_2}}{\bar{a}_2} \gamma\left(1 + \frac{m_2}{2}, \left(\frac{S_0}{2\sqrt{2m_{0ij}}}\right)^2\right)\right]$$

[47]

where $\bar{a}_1$, $\bar{a}_2$, m_1, and m_2 are parameters of two-slope SN curve and S_0 is stress range at which the slope of SN curve changes. Two kinds of incomplete gamma function are used.

4. Frequency Domain Method with Stretching Effect

There are two effects that affect fatigue damage; motion effect due to motion of structure and stretching effect due to wave elevation. In spectral method, introduced in section 3, nonlinearity caused by

Morison force can be taken into account using linearization coefficient. However, motion and stretching effects cannot be considered when calculating fatigue damage. It makes a difference between the results obtained by spectral method and the results by RFC method. Therefore, spectral method considering the effects is suggested in section 4. In this research, only stretching effect is included since stretching effect has a larger impact on fatigue than motion effect. The basis for this assertion is described in section 7.1.

4.1. Comparison of Spectral Method and Spectral Method with Stretching

Total local hotspot stress RAO can be obtained by summing up all local hotspot stress contributions below MWL if wave elevation is not considered (see Fig. 7 (a)). In spectral method introduced in section 3, no wave is assumed. However, if wave elevation is taken into account, local hotspot stress contributions below free surface should be combined when obtaining total local hotspot stress RAO. In addition, total local stress RAO differs when wave crest comes and wave trough comes (see Fig. 7 (b)). In spectral method with stretching, it is assumed that there is wave. It means the difference between spectral method and spectral method with stretching is existence of wave.

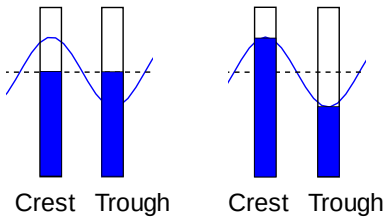

Fig. 7 Submerged range when there is (a) no wave (b) wave

4.2. Total Local Stress RAO Considering Stretching Effect

When considering the existence of wave, key point is the height to be added. In time domain, the height is wave elevation at each time step (see blue dash line in Fig. 8). However, in frequency domain, only one height should be chosen. In this study, the height is called characteristic wave amplitude, A_{added} (see green dash line in Fig. 8).

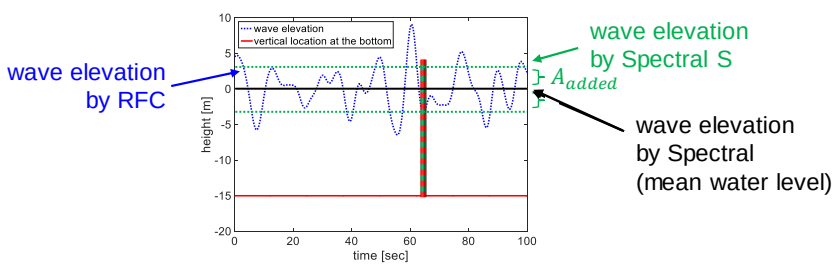

Fig. 8 Wave elevation by three different methods

Wave amplitude which is used for stretching can be explained using Fig. 9 easily. Fig. 9 (a) and (b) show wave amplitude for stretching in RFC method and spectral method with stretching,

respectively. In RFC method, stretching method can be applied differently according to different wave with small amplitude or large amplitude. However, in spectral method with stretching, stretching method should be applied using identical wave amplitude for different wave. It is limitation of spectral method with stretching and the wave amplitude is characteristic wave amplitude.

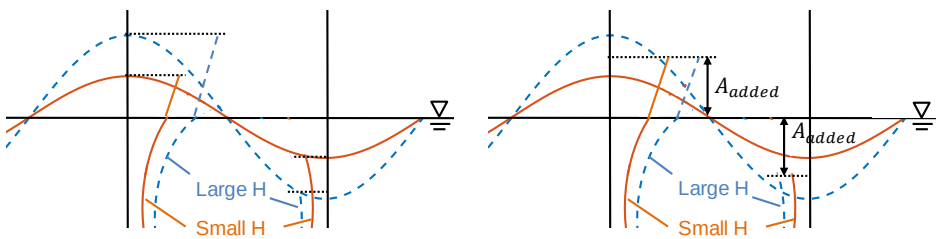

(a) (b)

Fig. 9 Wave amplitude for stretching in
(a) RFC method (b) spectral method with stretching

Characteristic wave amplitude should be the value that represents irregular wave well. The possible candidates for this value are the four wave amplitudes that are commonly used in water wave mechanics (presented in Eq.[48]). The concept of four wave heights can be seen in Fig. 10. Wave amplitude is half of wave height.

$$A_{most\ probable},\ \bar{A} = 1.25\sqrt{m_0},\ A_s = 2\sqrt{m_0},\ \bar{A}_{1/10} = 2.55\sqrt{m_0} \quad [48]$$

where $A_{most\ probable}$ is most probable wave amplitude, $\bar{A}$ is mean wave amplitude, A_s is significant wave amplitude, $\bar{A}_{1/10}$ is amplitude

of the highest 10% of waves.

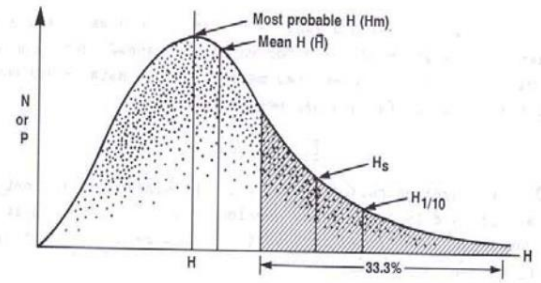

Fig. 10 Statistical distribution of wave heights showing various parameters

Once characteristic wave amplitude is determined, obtain total local stress RAO when crest and trough of that amplitude come and average two RAOs. The method which calculates fatigue damage in frequency domain using the averaged total local stress RAO is defined as spectral method with stretching in this research.

Difference in Stress profile for spectral method and spectral method with stretching is presented in Fig. 11. In spectral method, stress is applied to structure below MWL both when wave crest comes and when wave trough comes since wave elevation is not considered as described in Fig. 11 (a). In spectral method with stretching, wave elevation can be taken into account. Thus, stress is applied to structure below free surface when wave comes as described in Fig. 11 (b).

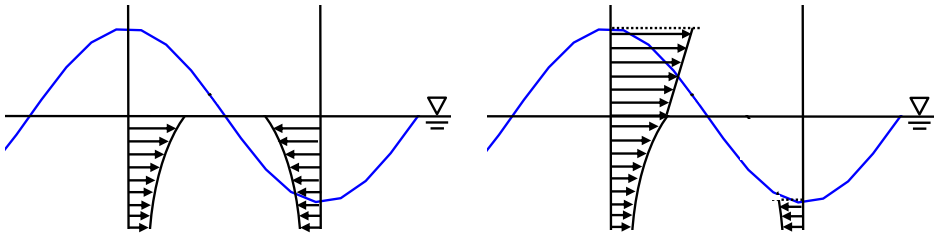

(a) (b)

Fig. 11 Stress profile for
(a) spectral method (b) spectral method with stretching

Stress range is range between stress when wave crest comes, σ_{crest}, and stress when wave trough comes, σ_{trough} (see Fig. 12 (a)). $\sigma_{average}$ can be obtained using the following equation.

$$\sigma_{average} = \frac{\sigma_{crest} - \sigma_{trough}}{2}$$

[49]

$\sigma_{average}$ in Fig. 12 (b) is stress RAO for spectral method. In spectral method, magnitude of σ_{crest}, σ_{trough}, and $\sigma_{average}$ is identical.

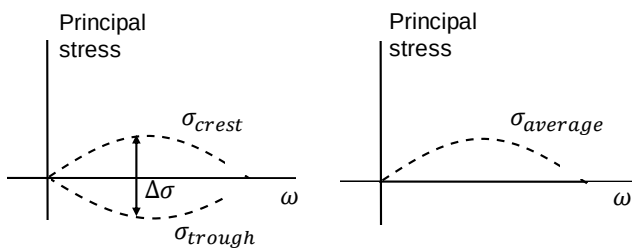

(a) (b)

Fig. 12 Stress range and stress RAO for spectral method

Fig. 13 (a) and (c) show stress range and (b) and (d) show stress RAO for spectral method with stretching. Fig. 13 (a) and (b) corresponds to the case where stress RAO is increased when considering stretching effect, defined as case 1. Fig. 13 (c) and (d) corresponds to the case where stress RAO is decreased when considering stretching effect, defined as case 2. In Fig. 13, $\sigma_{average}$ is stress RAO for spectral method (dash line) and $\sigma'_{average}$ is stress RAO for spectral method with stretching (solid line). As can be seen in Fig. 13 (a) and (c), stress is increased when wave crest comes and it is decreased when wave trough comes.

In case 1, increase in stress RAO caused by crest is greater than decrease due to trough. For this reason, stress range is increased when stretching effect is included and as a result, averaged stress RAO is increased. On the other hand, in case 2, decrease in stress RAO caused by wave trough is greater than increase due to crest. Thus, when stretching effect is considered, averaged stress RAO is decreased.

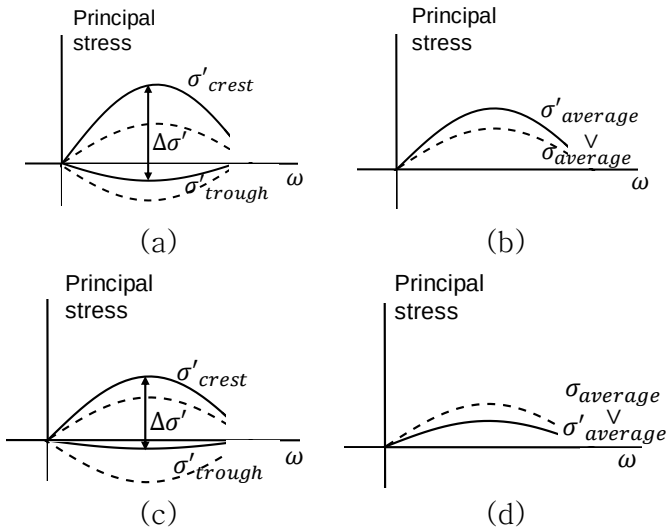

Fig. 13 Stress range and stress RAO for spectral method with stretching

5. Model Description

5.1. Global Model and Local Model

A barge-shaped FPSO with a vertical tube is used for the verification of the method proposed in this study. Fig. 14 (a) represents a panel model and the Morison model used in the hydrodynamic analysis. The same model is used as a global structural model. The vertical tube is located at the midship and supported by two brackets at the top and the bottom of the tube. The end of the bracket is rounded to mitigate stress concentration. Length, breadth, and height of the barge model are 280m, 32m, and 25m, respectively. Diameter and height of the vertical tube are 1m and 25m, respectively. Fig. 14 (b) and (c) show the top and bottom part of the vertical tube

with the supporting brackets. The tube is attached at only the positive y side (starboard). The origin of the barge model is located at the center of bottom plate.

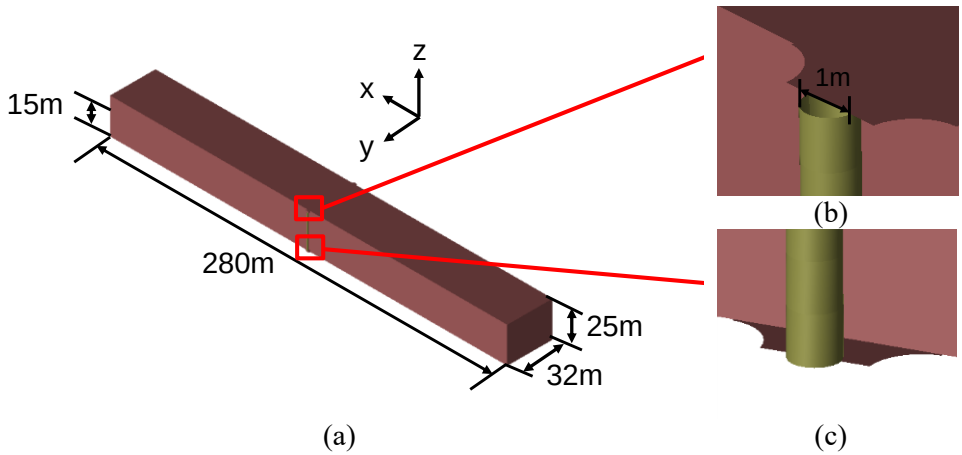

Fig. 14 A barge-shaped model
(a) global model (b) top part (c) bottom part of the tube

Fig. 15 illustrates a local FE model that includes the tube and two brackets connecting the tube to side shell. Two hotspot points are selected at the middle of the free edge of the top and bottom brackets. As depicted in Fig. 15 (a), two bracket parts are modeled with t x t shell elements.

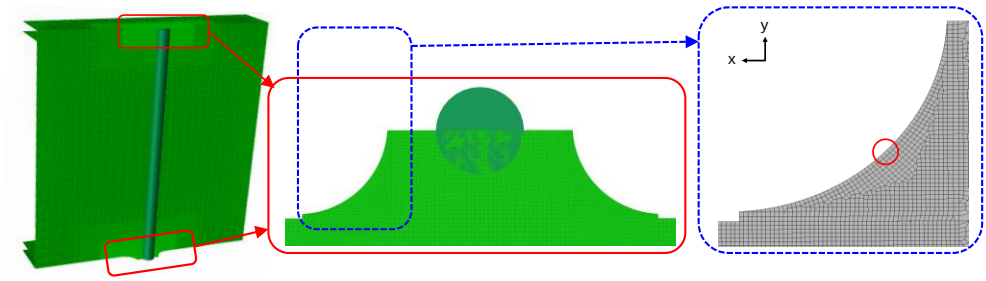

Fig. 15 A local model
(a) entire FE fine mesh (b) bracket part (c) hotspot point

Fig. 15 (b) and (c) show a fore side of the bracket and a hotspot point at the middle of bracket's free edge, respectively. Eight-node elements are used for the FE model. The hotspot points are intentionally selected, since the points are affected by both global hull girder load and, to some degree, the Morison load. The toe end of bracket on the side shell might be more prone to fatigue failure due to a larger hull girder load the free edge; however, the effect of the Morison load would be negligible. Global stress RAO and stress influence factors are calculated for the hotspot points at the free edge. For the calculation of global stress RAO, drag coefficient (C_D) and added mass coefficients (C_A) are set zero to remove the Morison load effect.

5.2. Motion Analysis and Fatigue Analysis Description

The global model introduced in 5.1 is used for the hydrodynamic analysis using WADAM (DNVGL, 2013a). Basic information for the analysis is specified below.

- Model type: composite model (panel model and Morison model)
- Angular frequency: from 0.165 to 1.615 at 0.05 interval [rad/sec]
- Heading angle: from 0 to 315 at 45 interval [deg] with equal occurrence probability (0.125)
- Added mass coefficients, $C_A = 100.0$ and drag coefficient, $C_D = 100.0$
- Draft: 15 [m]
- Water density: 1025 [kg/m^3]
- Water depth: 300 [m]

Definition of heading angles is illustrated in Fig. 16.

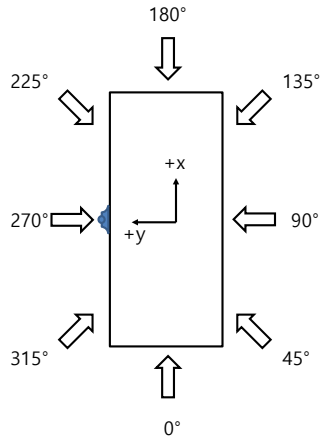

Fig. 16 Heading angles

Fluid particle velocity RAOs are extracted around the vertical tube at each depth. The particle velocity includes incoming wave velocity, diffracted wave velocity, and radiated wave velocity. That is, it is calculated from all of incident potential, radiation potential, and diffraction potential.

In what follows, further detail on the fatigue analysis is provided.

- Analysis time: 3 [hours]
- Design life: 20 [years]
- SN curve: C-curve with Cathodic Protection, $m_1 = 3$, $log\, a_1 = 12.192$, $m_2 = 5$, $log\, a_2 = 16.32$ (DNVGL, 2010, DNV-RP-C203)

- The number of wave seeds in irregular wave: 640
- Time step: 0.25 [sec]
- Used code: RFC code
- Wave spectrum: PM spectrum
- Wave scatter data: DNV−WW with 142 sea states
- Stretching method: vertical stretching, extrapolation stretching

5.3. Drag and Added Mass Coefficient Selection

There are two kinds of coefficients in the Morison equation: drag coefficient (C_D) and inertia coefficient (C_M). In WADAM, drag coefficient and added mass coefficient (C_A) should be given. The relationship between inertia coefficient and added mass coefficient is defined by the following formula:

$$C_M = 1 + C_A$$

[50]

Normally, drag coefficient for a vertical tube subjected to linear waves has been reported to be about 1~1.4 and added mass coefficient is 1. In the present study, local hotspot stress is much smaller than global stress due to the small slenderness of the tube.

The key point of this paper is finding appropriate linearization coefficient to express nonlinear Morison load well. However, in the case that global stress is much bigger than local stress, the effect of linearization coefficient is hard to be found. To observe the effect caused by the usage of linearization coefficient clearly, local stress should be as large as global stress. For this reason, a value of 100.0 is used for both the drag and the added mass coefficients to make the orders of local hotspot stress and global stress similar.

5.4. Stress Influence Factor

Stress influence factors are computed by imposing a unit load at 25 points along the caisson one by one and measuring three stress components ($\sigma_x, \sigma_y, \tau_{xy}$). The tube of 25m height is divided into 25 segments and the unit load is separately applied at the center of each segment in x and y directions. Therefore, a total of 150 factors are defined (3x25x2=150) for one hotspot point. Fig. 17 (a) shows hotspot points and Fig. 17 (b) examples of imposing unit load at certain locations.

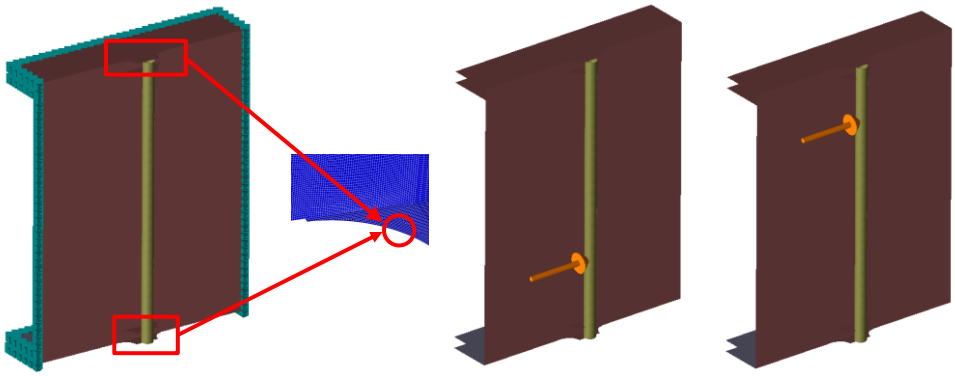

(a) (b)

Fig. 17 (a) hotspot points (b) unit load application to each location

6. Results for Frequency Domain Method

6.1. Verification of In-house Code

Fatigue damage can be computed using three methods: (1) frequency domain code using the spectral method (called spectral code hereafter); (2) time domain code using the RFC method (called RFC code hereafter); (3) and DNV-STOFAT (DNVGL, 2014).

Verification of in-house code is performed using DNV-STOFAT. The following three assumptions used in STOFAT are applied in the code as well to compare with STOFAT.

- Incident wave kinematics is applied.
- Following linearization method is used.

$$F = \rho V C_M a + \frac{1}{2}\rho C_D A u \frac{8}{3\pi} V_{max} \quad (V_{max} = 2m/s)$$

- There are no motion of structure and wave elevation considered.

In the first assumption, incident wave kinematics means wave kinematics obtained under the condition where radiation and diffraction effects are not taken into account.

6.1.1. Verification of Spectral Code

There are two types of fatigue damage; fatigue damage induced by global stress and combined stress. The fatigue difference between spectral code and STOFAT is found to be quite small for the case of global stress (see Table 2). However, there is a difference in the comparison of fatigue damages by combined stress. The difference occurs due to the inequality of input data; incident wave kinematics.

When the Morison force is calculated in WADAM, two types of particle velocities can be used: one considering all of incident, diffracted, and radiated waves and the other considering only incident wave. For a floating structure, WADAM provides the Morison load calculation only for incident wave. Thus, in order to compare with the fatigue damage calculated based on the incident wave kinematics in STOFAT, incident wave particle velocities are needed for the RFC code. However, WADAM serves velocities calculated from incident, radiation, and diffraction potentials as output. Thus, incident wave kinematics is obtained from the hydrodynamic analysis for an

extremely small floating box panel model to minimize the effect of diffraction and radiation. For this reason, there is a difference in the output results since there is a difference in the input data.

Table 2 Fatigue damage obtained by spectral code and STOFAT

Type of stress	Spectral code	STOFAT	Difference [%]
Global stress	27.84	27.78	0.22
Combined stress	51.81	53.85	−3.80

It is concluded that spectral code is verified through the small difference of the results despite the fact that there is a difference of input.

6.1.2. Verification of RFC Code

Verification of spectral code is completed in 6.1.1. Verification of RFC code is conducted using spectral code since both code use identical input data; incident wave kinematics.

Fatigue damages calculated by RFC code and spectral code are shown in Table 3. The results from RFC code are smaller than those from spectral code. It is consistent with the fact that RFC method is generally known to give a smaller fatigue than spectral method. The difference in the case of global stress is caused by the RFC effect. The difference in the case of combined stress occurs due to the

combination of RFC effect and the difference of input data. Verification of RFC code is finished.

Table 3 Fatigue damage obtained by RFC code and spectral code

Type of stress	RFC code	Spectral code	Difference [%]
Global stress	26.52	27.84	−4.73
Combined stress	49.07	51.81	−5.30

6.2. Results for Linearization Coefficient

6.2.1. Computational Time

To calculate total fatigue damage for 8 heading angles and 142 sea states, it takes 37 hours and 9 minutes by RFC code and spectral code, respectively. Computational time by RFC code is 248 times bigger than that by spectral code.

6.2.2. Results for Local Stress

In this section, comparison of the results obtained under the same conditions, no motion effect and no stretching effect considered, except for the use of linearization coefficient is conducted to verify the accuracy of the linearization coefficient. Three types of fatigue calculation methods are defined in Table 4 to perform the verification of linearization coefficient.

Table 4 Classification of three methods for verification of linearization coefficient

	Spectral W	Spectral N	RFC
Type of Morison force	Linearized (wide-band)	Linearized (narrow-band)	Nonlinear
Motion effect	X	X	X
Stretching effect	X	X	X

Fatigue damages by three methods for local stress are shown in Table 5. To check the effect by the use of linearization coefficient purely, RFC effect is removed by applying −5.3% as RFC correction factor to the results calculated by spectral W and spectral N. Modified results can be seen in Fig. 18. In both brackets, there is little difference between spectral and RFC results.

Table 5 Fatigue damage obtained by three methods for local stress

Bracket	Spectral W	Spectral N	RFC
Lower	7.48	7.51	7.15
Upper	2.79	2.81	2.70

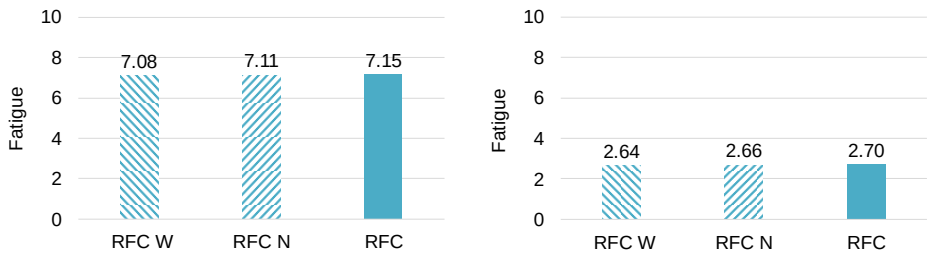

Fig. 18 Modified fatigue damage obtained by three methods for local stress (a) for lower bracket (b) for upper bracket

6.2.3. Results for Combined Stress

Fatigue damages by three methods for combined stress are shown in Table 6. RFC effect is taken into account. Modified results can be seen in Fig. 19. There is little difference between spectral and RFC results as well for combined stress.

Table 6 Fatigue damage obtained by three methods for combined stress

Bracket	Spectral W	Spectral N	RFC
Lower	49.62	49.69	51.31
Upper	7.97	7.99	7.69

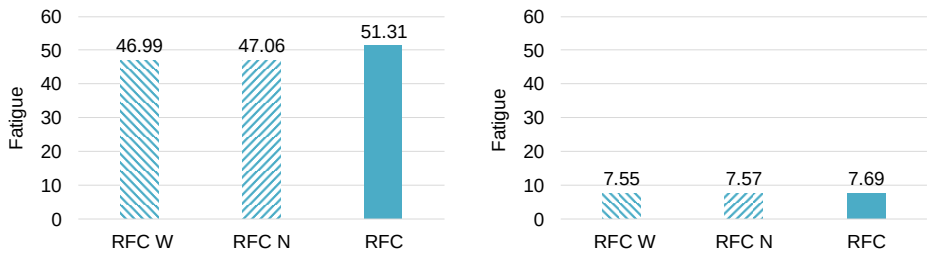

Fig. 19 Modified fatigue damage obtained by three methods for combined stress (a) for lower bracket (b) for upper bracket

Through the results from 6.2, it can be seen that linearization method used in this research shortens the analysis time and approximate nonlinear Morison force well.

One more thing to note here is that two different linearization coefficient calculation methods yield almost the same results. Case

studies are performed in 6.3 to find the reason.

6.3. Comparison between Narrow-band Method and Wide-band Method

6.3.1. Case Study for Ochi-Hubble Spectrum

First case study is conducted using Ochi−Hubble spectrum which has two−peaks. Ochi−Hubble spectrum is made by the combination of two one−peak spectra. It is defined by two H_s, T_p, λ. Here, T_p is peak to peak period and λ is shape parameter. Ochi−Hubble spectrum is expressed by the following equation.

$$S(f) = S_1(f) + S_2(f)$$

$$S_i(f) = \frac{\pi}{2} \cdot \frac{\left\{4 \cdot (4\lambda_i + 1) \cdot \pi^4 \cdot {fp_i}^4\right\}^{\lambda_i}}{\Gamma(\lambda_i)} \cdot \frac{{Hs_i}^2}{(2\pi f)^{4\lambda_i+1}} \cdot exp\left[-\frac{4\lambda_i + 1}{4} \cdot \left(\frac{fp_i}{f}\right)^4\right]$$

[51]

where $S(f)$ is Ochi−Hubble spectrum, $S_i(f)$ is one−peak spectrum, and f is frequency [1/sec].

There are six cases where both T_{p_1}, T_{p_2} are different. Fatigues are calculated by two methods and the results are presented in Fig. 20. It can be seen that there is no difference between two methods in all cases.

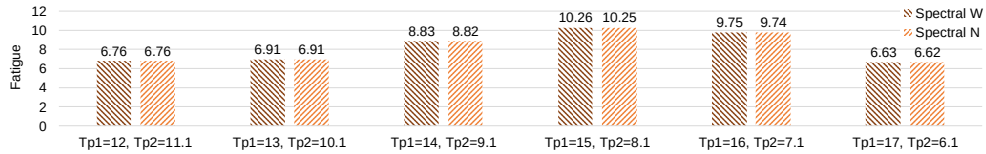

Fig. 20 Fatigue damage obtained by two methods for OH spectrum

The reason can be found from the comparison of bandwidth parameter of wave and stress spectrum illustrated in Fig. 21.

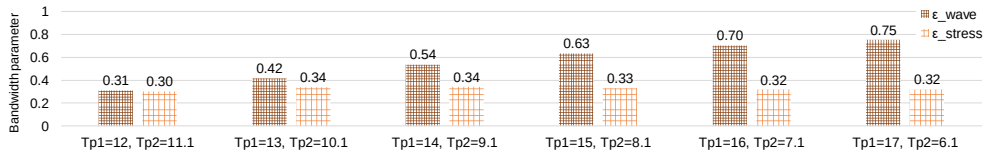

Fig. 21 Bandwidth parameter of wave and stress spectrum for OH spectrum

Wave, force, and stress are linearly related since Morison force is linearized using linearization coefficient. Therefore, linearization method that can be applied when wave spectrum is wide-band or narrow-band can be thought of as a method that can be applied when stress spectrum is wide-band or narrow-band. For all cases performed in this case study, it can be seen that stress spectrum approaches narrow-band process even though wave spectrum is wide-band. For this reason, it is thought that the results obtained by two different linearization methods are almost identical.

In order to check spectral bandwidth change visually, one case

where the difference in bandwidth parameter is greatest, $T_{p_1} = 17sec$, $T_{p_2} = 6sec$, is chosen and wave spectrum, force spectrum, and stress spectrum for the case are compared. Fig. 22 (a), (b), (c) show wave spectrum, force spectrum, and stress spectrum, respectively. Here, force spectrum corresponds to force spectrum in the x direction at MWL. As can be seen in Fig. 22, spectral bandwidth decreases as wave spectrum becomes stress spectrum through force spectrum.

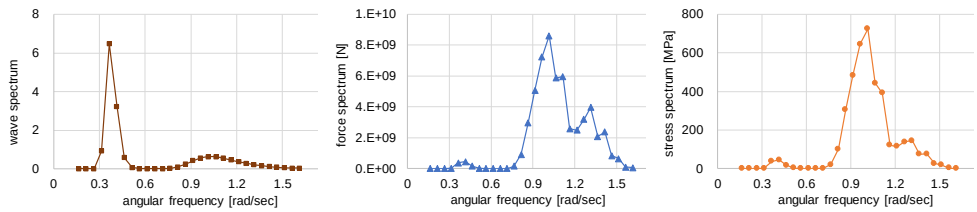

(a) (b) (c)

Fig. 22 Three spectrum comparison for OH spectrum
(a) wave spectrum (b) force spectrum (c) stress spectrum

6.3.2. Case Study for PM Spectrum

To double check this phenomenon, another case study is performed for PM spectrum which has one-peak. There are seven cases where significant wave height, H_s, is same and zero up-crossing period, T_z, is different. T_z is separated from 4.5 seconds to 10.5 seconds at 1 second interval. Fatigues are calculated by two linearization coefficient calculation methods, for wide-band and narrow-band wave spectrum and the results are presented in Fig.

23. It can be seen that there is no difference between two methods in all cases.

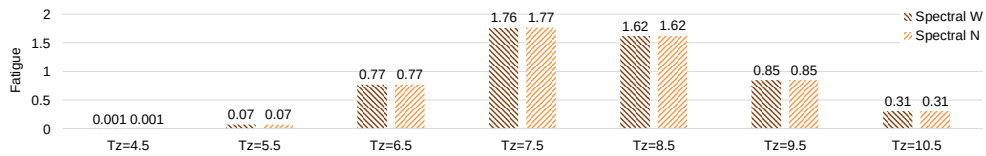

Fig. 23 Fatigue damage obtained by two methods for PM spectrum

The reason of identical results is same with that found in the case study for OH spectrum (see Fig. 24).

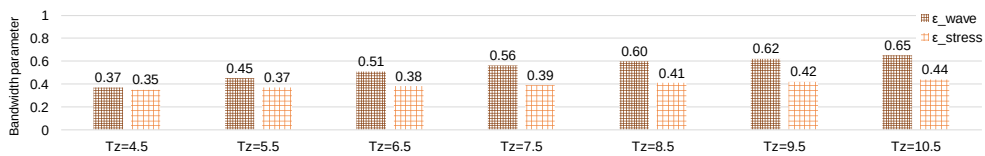

Fig. 24 Bandwidth parameter of wave and stress spectrum for PM spectrum

Wave spectrum, force spectrum, and stress spectrum are compared (see Fig. 25) for the case where the difference in bandwidth parameter is greatest, $T_z = 10.5sec$, as done for Ochi-Hubble spectrum (see Fig. 22). In the comparison for Ochi-Hubble spectrum, bandwidth difference of three spectra can be found easily, but it is difficult to check in that for PM spectrum.

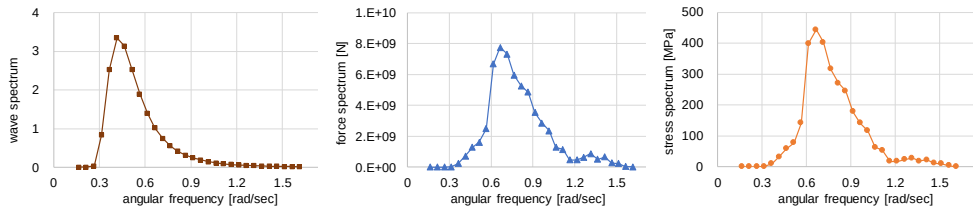

(a) (b) (c)

Fig. 25 Three spectrum comparison for PM spectrum
(a) wave spectrum (b) force spectrum (c) stress spectrum

7. Results for Frequency Domain Method with Stretching Effect

From the results of section 6, it is confirmed that the spectral method can serve similar results to the RFC method when there is no motion of structure and wave elevation considered. However, both factors exist in the actual situation. Therefore, to improve the accuracy of spectral method; first, find out which of the two factors is dominant, and then, propose a way to consider the factor in spectral method.

7.1. Results for Various Effects

There are two effects that affect fatigue damage; motion effect due to motion of structure and stretching effect due to wave elevation. The results calculated by four kinds of RFC method are compared to confirm only the motion and stretching effect purely except for RFC effect (see Table 7). In the table, the letter M means motion and S

means stretching. Both stretching method, vertical stretching and extrapolation stretching, are used to find the difference from the two stretching methods when calculating the results. To figure out the effect of motion and stretching on local stress, global stress is excluded in fatigue calculation.

Table 7 Classification of four methods to investigate the influence of various effects

	RFC	RFC M	RFC S	RFC MS
Type of Morison force	Nonlinear			
Motion effect	X	O	X	O
Stretching effect	X	X	O	O

7.1.1. Results for Vertical Stretching

Two facts can be seen in the figure below. The first is that stretching effect has a greater impact on fatigue than motion effect. The second is that stretching effect is greater in upper bracket, which is closer to the MWL, than lower bracket.

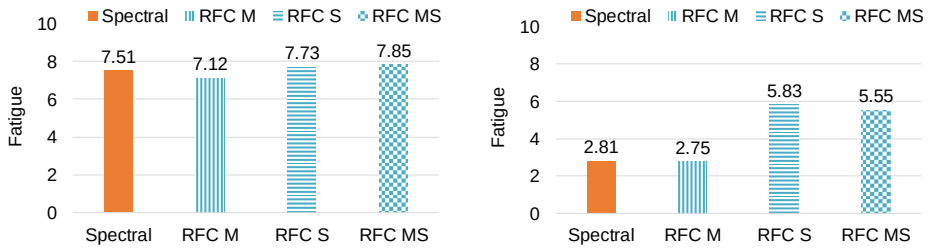

Fig. 26 Fatigue damage obtained by four methods using vertical stretching (a) for lower bracket (b) for upper bracket

7.1.2. Results for Extrapolation Stretching

The results calculated using vertical and extrapolation stretching show that stretching effect is larger when using extrapolation stretching than vertical stretching.

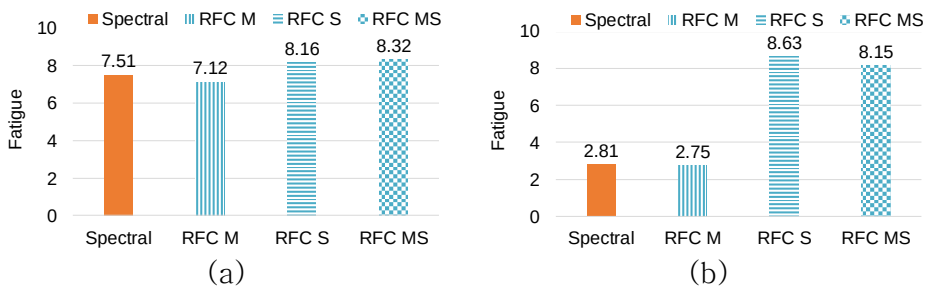

Fig. 27 Fatigue damage obtained by four methods using extrapolation stretching (a) for lower bracket (b) for upper bracket

From the results of section 7.1, it can be seen that the accuracy of spectral method can be improved if it can consider stretching effect in frequency domain. For this reason, frequency domain method with stretching effect, introduced in section 4, is suggested and the results

are presented in the next section (see section 7.2).

7.2. Results for Consideration of Stretching Effect

7.2.1. Results for Upper Bracket

Spectral method with stretching, described in section 4.2, is applied to upper bracket first where stretching effect is larger. Results are calculated using both vertical stretching and extrapolation stretching.

7.2.1.1. Results for Vertical Stretching

Even though four candidates that can be used as characteristic wave amplitude are introduced in section 4.2, ten wave amplitudes are used for more detailed comparison.

In Fig. 28, notation S indicates stretching. Spectral, Spectral S, RFC S means spectral method, spectral method with stretching, and RFC method including only stretching effect, respectively. Results obtained by spectral method and spectral S method are modified using RFC correction factor, −5.3%, to compare with the result by RFC S method.

Three things can be found in Fig. 28. The first is that results including stretching effect in frequency domain is closer to RFC results than the that not including the effect. The second is that the

larger wave amplitude is used, the larger fatigue is. It corresponds to the case 1 introduced in section 4.2. The third is that when $\overline{A_{1/10}}$ is used, the results that are most similar to the RFC results can be obtained. However, using amplitude larger than $\overline{A_{1/10}}$ has the potential to yield closer results to RFC results in the case of vertical stretching.

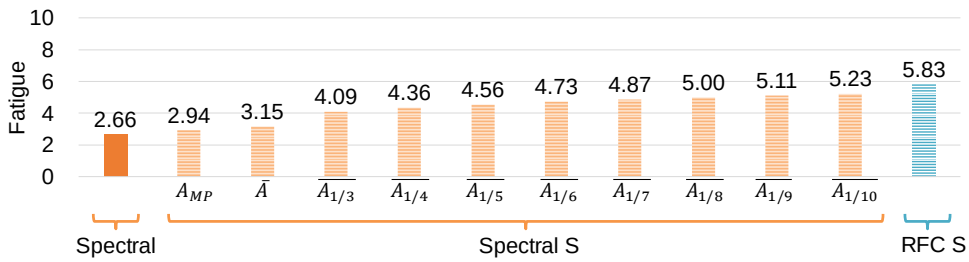

Fig. 28 Fatigue calculated considering stretching effect for upper bracket and vertical stretching

Fig. 28 shows fatigue sum for all sea states, and Fig. 29 shows fatigue for each sea state. X label of Fig. 29 is fatigue calculated by RFC S method and y label of Fig. 29 is fatigue obtained by spectral S method and modified using RFC correction factor.

When points are on a blue straight line with a slope of 1, it means the results obtained by two methods match. It can be found that most of the points are located near the straight line.

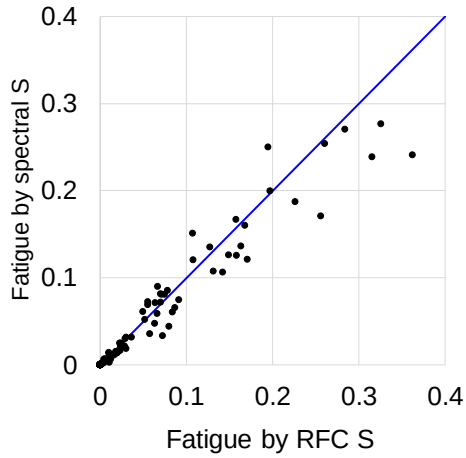

Fig. 29 Fatigue calculated considering stretching effect for upper bracket and vertical stretching at each sea state

7.2.1.2. Results for Extrapolation Stretching

In the case of extrapolation stretching, when $\overline{A_{1/8}}$ is used, the results that are most similar to the RFC results can be obtained. When comparing the results from both stretching methods, it can be seen that fatigue is more affected by stretching effect when extrapolation stretching is used.

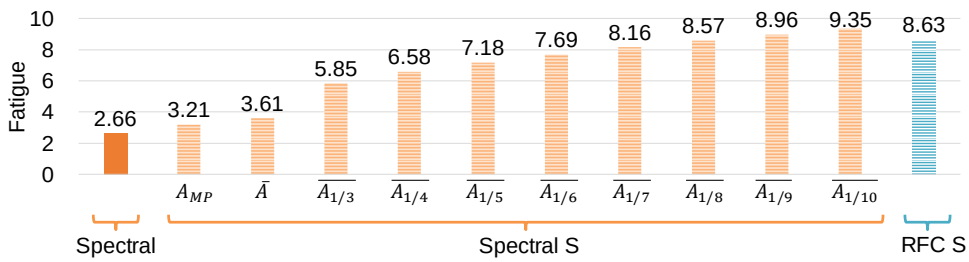

Fig. 30 Fatigue calculated considering stretching effect for upper bracket and extrapolation stretching

As in the case of using vertical stretching, it can be seen that most of the points are located near the straight line except for some points when extrapolation stretching is used.

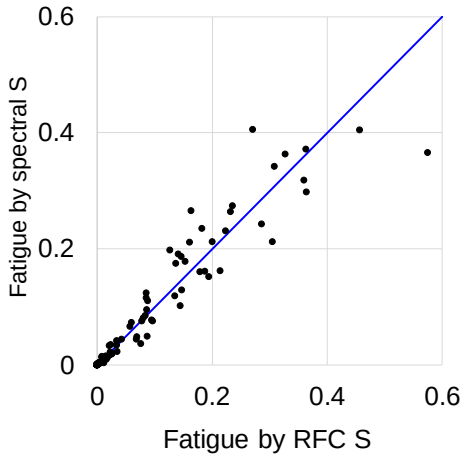

Fig. 31 Fatigue calculated considering stretching effect for upper bracket and extrapolation stretching at each sea state

Through the results from section 7.2.1, spectral method with stretching appears to give a decent result for the case of upper bracket.

7.2.2. Results for Lower Bracket

7.2.2.1. Results for Vertical Stretching

In order to double check the effectiveness of spectral method with stretching, the method is also applied to lower bracket. In this case, only four characteristic wave amplitudes are used. When looking at

the results obtained using vertical stretching for lower bracket (see Fig. 32), the results considering stretching effect is farther from RFC results than that not considering the effect. It is because that it corresponds to the case 2 described in 4.2.

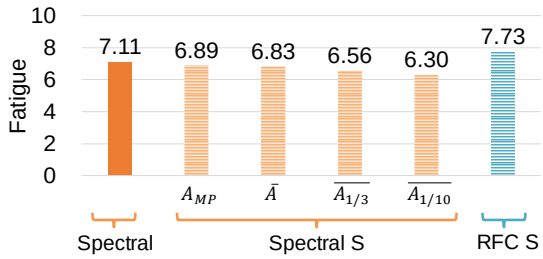

Fig. 32 Fatigue calculated considering stretching effect for lower bracket and vertical stretching

7.2.2.2. Results for Extrapolation Stretching

The results obtained by using extrapolation stretching for lower bracket show that stretching effect does not have a significant effect on fatigue damage. However, there is a possibility that fatigue becomes bigger when using larger wave amplitude.

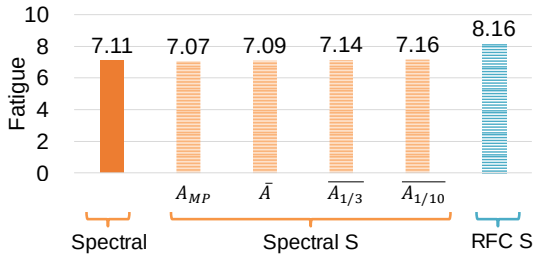

Fig. 33 Fatigue calculated considering stretching effect for lower bracket and extrapolation stretching

From the results of section 7.2, spectral method with stretching appears to be effective to some degree for hotspot points adjacent to intermittent zone, which means the area close to MWL, but not for points far from the zone. Furthermore, even for hotspot points near intermittent zone, there is no guideline how to select a proper characteristic wave amplitude. Therefore, it can be concluded that spectral method with stretching needs further improvement.

8. Conclusion

8.1. Summary

In actual situation, there are three factors that make a difference between the results obtained by time domain method and frequency domain method; nonlinearity of Morison force, motion effect due to motion of structure, and stretching effect due to wave elevation. According to the factors, three kinds of method are developed in this

paper; time domain method, frequency domain method, and frequency domain method with stretching effect. Each method is called RFC method, spectral method, and spectral method with stretching, respectively in the research. In RFC method, nonlinearity of Morison force, motion of structure, wave elevation are taken into account. Thus, the results close to the exact solution can be obtained through RFC method. In spectral method, stochastic linearization coefficient calculation method is applied. Two types of linearization method are used; for narrow-band wave spectrum and wide-band wave spectrum. In case of linearization method for wide-band wave spectrum, PDF of peak force for wide-band spectrum is derived in this paper. In the spectral method with stretching, method that can consider stretching effect due to wave elevation is used when obtaining total local stress RAO.

8.2. Findings

Through various results analysis, our findings can be summarized in six categories. The first is that in the absence of motion and stretching effects, nonlinear Morison force can be well approximated by stochastic linearization coefficient. The second is that the main factor that makes the difference between spectral results and RFC results is stretching effect. The third is that decent results can be

obtained using spectral method at the hotspot points far from the intermittent zone where stretching effect is small. The forth is that it is recommended to use RFC method at the points adjacent to the intermittent zone to properly consider stretching effect since it is large in that zone. The fifth is that if conservative value such as $\overline{A_{1/10}}$ as characteristic wave amplitude is used, spectral method with stretching can also be used in the intermittent zone. The last is that two spectral methods can reduce computational time for the analysis dramatically.

Reference

[1] Borgman, L.E., 1972. Statistical models for ocean wave forces. Advances in hydroscience. 8, pp. 139-181.

[2] Bretschneider, C.L., 1964. The generation of waves by wind: state of the art. Office of Naval Research. pp. 1-96.

[3] Brouwers, J.J.H, Verbeek, P.H.J., 1983. Expected fatigue damage and expected extreme response for Morison-type wave loading. Probabilistic offshore mechanics. pp. 97-101.

[4] Choi, Y.H., Kwon, S.H., Kim, D.W., Park, S.K., 1995. A Reliability study of coastal structures under the influence of waves and currents – Random Analysis of Fixed Structures. Journal of Ocean Engineering and Technology. 9 (2), pp. 186-192.

[5] DNVGL, 2010, Fatigue design of offshore steel structures, DNV Recommended Practice C203, Det Norske Veritas AS.

[6] DNVGL, 2014, SESAM user manual sestra(2013), Det Norske Veritas, Norway.

[7] DNVGL, 2014, SESAM user manual stofat(2014), Det Norske Veritas, Norway.

[8] DNVGL, 2013a, SESAM user manual wadam(2013), Det Norske Veritas, Norway.

[9] Karadeniz, H., 1994. Linear and nonlinear response analyses of offshore structures under random wave and current loading. Proc. of the 4th Intl. Offshore and Polar Eng. Conf., Osaka, Japan, pp. 328-333.

[10] Moe, G., Crandall, S.H., 1978. Extremes of Morison-type wave loading on a single pile. Journal of Mechanical Design. 100, pp. 100-104.

[11] Price, W.G., 1974. Probability theory of ship dynamics. Chapman and Hall. p.170.

[12] Tickell, R.G., 1977. Continuous random wave loading on structural members. The Structural Engineer. 55, pp. 209-222.

[13] Tung, C.C., 1974. Peak distribution of random wave-current force. Journal of the Engineering Mechanics Division. EM5, pp. 873-884.

[14] Wheeler, J.D., 1969. Method for calculating forces produced by irregular waves. Journal of Petroleum Technology. Proc. of Offshore Technology Conference. Houston, USA, pp. 71-79.

초록

수직 튜브에 작용하는 모리슨 하중의 비선형성을 고려한 피로 해석에 관한 연구

모리슨 하중을 받는 해양 구조물에는 싱글 파일 형태의 구조물과 싱글 파일들의 복합체인 멀티 파일 구조물이 있다. 그 중 수직 싱글 튜브인 FPSO에 부착되어 있는 해수 케이슨을 본 연구의 대상으로 선정하였다. 해수 케이슨에서의 피로 파괴는 케이슨 자체에서보단 케이슨과 FPSO 선체의 접합부에서 많이 발생하기 때문에, 케이슨에 대한 피로 해석은 접합부에서 수행되어야 한다. 케이슨의 접합부는 모리슨 하중에 의한 국부 핫스팟 응력뿐만 아니라 헐 거더 하중에 의한 전선 핫스팟 응력을 동시에 받기 때문에, 접합부에서의 피로 해석을 수행할 때 두 응력을 함께 고려해야 한다. 또한, 모리슨 하중의 항력 성분에는 속도 제곱에 의한 비선형성이 존재하기 때문에, 피로 해석 수행 시 모리슨 하중의 비선형성도 고려해야 한다.

실제 상황에서는 FPSO와 같은 부유식 해양 구조물에 대해 피로 해석을 수행할 때, 모리슨 하중의 비선형성뿐만 아니라 구조물의 운동과 파에 의한 영향도 고려해주어야 한다. 주파수 영역 해석 방법과는 달리 시간 영역 해석 방법에서는 앞에서 언급한 모든 요소들이 다 고려될 수 있다. 이 때문에 시간 영역 해석 방법의 결과는 정확도가 높지만 해석

시간이 길다는 단점이 있다. 따라서 두 방법의 장점들을 적절히 가지고 있는 방법을 개발하기 위해서 본 연구를 시작하게 되었다.

본 연구에서는 한 가지의 시간 영역 해석 방법과 두 가지의 주파수 영역 해석 방법 절차 및 코드를 개발하였다. 본 연구에서 RFC 방법이라고 칭해지는 시간 영역 해석 방법은 모든 요소들을 고려할 수 있기 때문에 정해와 가장 가까운 해를 구할 수 있다. Spectral 방법이라고 불리는 첫 번 째 주파수 영역 해석 방법은 모리슨 하중의 비선형성만 반영할 수 있으며, Stretching을 포함한 spectral 방법이라고 불리는 두 번 째 주파수 영역 해석 방법에서는 파의 존재에 의한 stretching 효과를 고려하기 위한 시도가 수행되었다.

시간 영역 해석 방법에서는 수면 위에서는 상대속도를 구하기 위해 vertical stretching, extrapolation stretching 두 가지의 stretching 방법을 사용하였다. 또한, 각 높이 별 상대 속도 간의 관계를 유지하기 위해서 중첩법을 적용하였으며, 시간에 따라서 변화하는 구조물의 침수 면적에 대한 고려도 포함되었다. 주파수 영역 해석 방법에서는 협대역 파 스펙트럼과 광대역 파 스펙트럼에 대해 사용할 수 있는 두 가지 선형화 방법을 사용하여 선형화계수를 구하였다. 뿐만 아니라, stretching 방법을 사용하여 stretching 효과를 고려하기 위한 시도가 수행되었다.

결과 파트는 크게 5가지 카테고리로 분류할 수 있다. 첫 번째 카테고리에서는 상용 프로그램을 사용하여 본 연구에서 개발한 코드를 검증하였다. 다음으로, 개발한 코드를 사용하여 선형화계수가 비선형

모리슨 하중을 얼마나 잘 근사하는지를 확인하였으며, 두 가지 선형화 방법을 비교하였다. 남은 두 카테고리는 stretching을 포함한 spectral 방법을 검증하기 위해 수행되었다. 먼저, motion 효과와 stretching 효과 중에 어느 요소가 피로 손상도에 더 큰 영향을 미치는지 파악하고, 그 다음에 그 효과를 고려하여 새롭게 제안한 방법의 유효성을 검증하였다.

주요어 : Fatigue analysis, Vertical tube, Nonlinearity of Morison force, Stretching effect, Time domain method, Frequency domain method, Stochastic linearization coefficient

학 번 : 2015-21158